

# Strategies for assessing Early–Middle (Pliensbachian–Aalenian) Jurassic cyclochronologies

BY LINDA A. HINNOV<sup>1</sup> AND JEFFREY J. PARK<sup>2</sup>

<sup>1</sup>*Department of Earth and Planetary Sciences, Johns Hopkins University,  
Baltimore, MD 21218, USA*

<sup>2</sup>*Department of Geology and Geophysics, Yale University,  
New Haven, CT 06520, USA*

There are a number of fundamental problems in assessing the astronomically forced cyclostratigraphy of the Jurassic Period. First, Jurassic geochronology is not well constrained, due to a general scarcity of radiometric dates, inferior precision of the existing ones, and large inaccuracies in stratigraphic constraints. These problems are particularly troublesome in the Early to Middle Jurassic cyclic carbonates of the Colle di Sogno section in the Lombardy Pre-Alps, Italy. Second, Jurassic sedimentary formations have undergone significant diagenesis, and again, the Colle di Sogno carbonates, with their location on the southern edge of the Alpine fold belt, are no exception. This prevents the recovery of the primary geochemical proxies needed to evaluate the relationship between cyclic sedimentation and orbital forcing. Finally, even when a strong case can be made for orbitally forced cycles, a direct calibration between the Jurassic and existing theoretical orbital solutions is not yet possible. However, at Colle di Sogno new nannofossil biostratigraphy provides the opportunity to make significant headway in recognizing Jurassic signals consistent with orbital theory, and to propose cyclochronological estimates for a portion of the Pliensbachian, and for the combined Toarcian–Aalenian Stages. We evaluate the presence of orbital signals in the sequence through the use of frequency modulation analysis of the cycles, as well as by spectral analysis of lithologic rank time-series reconstructions. The results show that the Pliensbachian Domaro Limestone contains a dual-component precession-like signal that undergoes frequency variation indicative of modulation by orbital eccentricity. The signal subsequently evolves into a single-component signal with frequency perturbations similar to those of the obliquity variation in the overlying Toarcian–Aalenian Sogno Formation. This switch in response to the fundamental orbital modes occurs during the deposition of the Lower Toarcian black shale, a time of significant global environmental change. The biostratigraphy at Colle di Sogno has well-defined Pliensbachian–Toarcian and Toarcian–Aalenian boundaries, allowing a cyclochronologic minimum estimate of  $11.37 \pm 0.05$  ( $1\sigma$ ) Ma for the duration of the Toarcian–Aalenian interval (not accounting for stratigraphic and taxonomic noise). This compares well with the  $13.1 \pm 2.8$  ( $1\sigma$ ) Ma estimated for this same stratigraphic interval using the current radiometric geochronology. The underlying precession-forced Pliensbachian Domaro Limestone limestone–shale couplets suggest a time of formation for the sequence of least 5 Ma, with an age of onset in the *jamesoni* or *polymorphus* subzone.

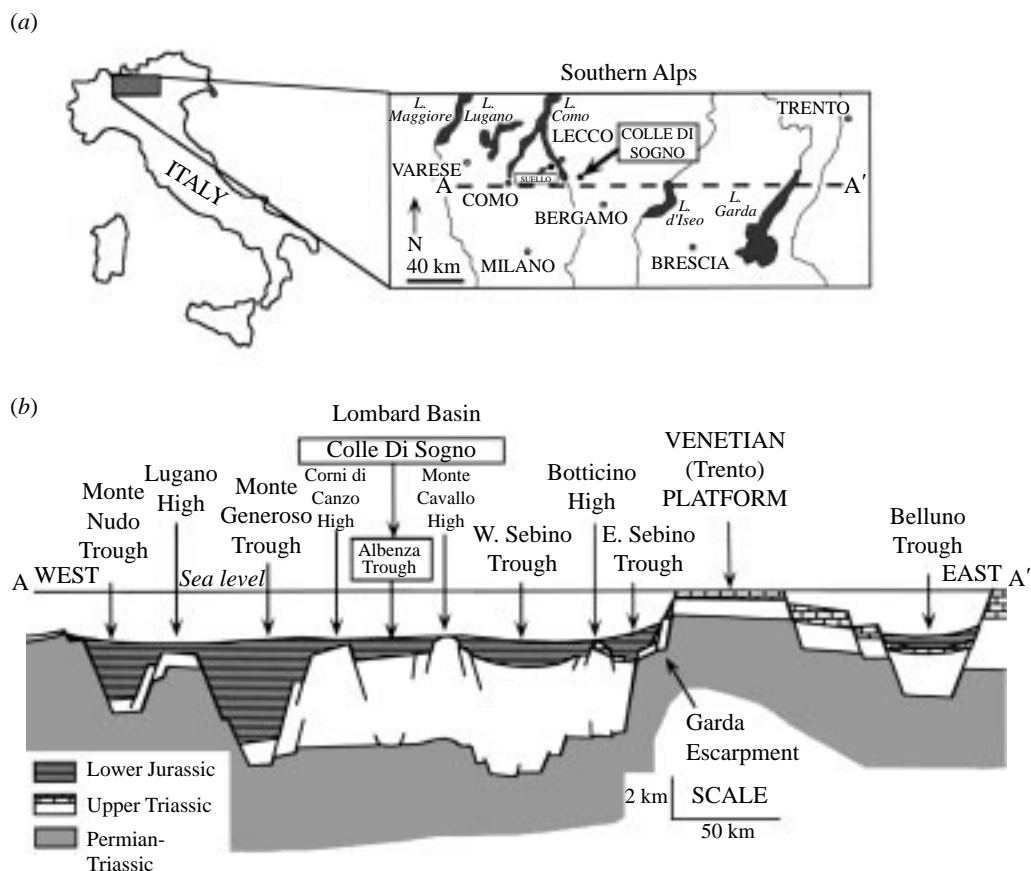
**Keywords:** Jurassic; cyclostratigraphy; chronostratigraphy; orbital forcing; palaeoclimate; frequency modulation

## 1. Introduction

The recognition of orbital signals in Jurassic marine cyclostratigraphy has been impeded by imprecise radiometric geochronometry, poorly defined stage boundaries due to provincialism and diachronism in the Jurassic fossil record, and diagenesis that tends to affect older sedimentary formations. Imprecise geochronometry results in inadequately constrained estimates of cyclostratigraphic frequency modes; uncertain stage boundary definitions compound this problem when correlating established geochronology to local stratigraphies. Diagenesis prevents recovery of primary palaeoenvironmental signals needed to evaluate the connections among orbital insolation forcing, climatic response, and the depositional record. Despite these problems, it is still possible to make preliminary evaluations of the presence of orbital signals in some Jurassic cyclostratigraphic sequences, and to develop provisional cyclochronologies, as proposed here, as well as previously by Van Buchem *et al.* (1994), Weedon & Jenkyns (1999) and Weedon *et al.* (this issue) over other Jurassic intervals.

Geochronology constrains the timing of thin bedded sedimentary cycles to the Milankovitch frequency band (although not always to a particular mode), thus from the outset a hypothesis of orbital forcing may be tested. If a number of basic criteria can be satisfied, then the presence of orbital signals can be inferred and a cyclochronologic estimate can be made on a provisional basis, subject to validation by a reassessment of the geochronology. The now classic example of this is the cyclochronologic challenge by Johnson (1982) and again by Shackleton *et al.* (1990), who, by counting orbital cycles, predicted that the established Matuyama–Brunhes boundary radioisotope date of  $730 \pm 11$  ka ( $1\sigma$ ; uncertainties are reported at the  $1\sigma$  level throughout the paper) (Mankinen & Dalrymple 1979) was underestimated by 5–7%. Subsequent reanalyses of this date confirmed this with new Ar–Ar dates of  $780 \pm 10$  ka (Spell & McDougall 1992) and  $790 \pm 6$  ka (Berger *et al.* 1995). Of course, this method of ‘checks and balances’ can also bring into question Milankovitch interpretations of stratigraphy, as for example the recent high-precision U/Pb zircon dating by Brack *et al.* (1996) of the Middle Triassic Latemar Limestone (Goldhammer *et al.* 1987, 1990), although the accuracy of those zircon dates has been questioned by Hardie & Hinnov (1997) (see also Brack *et al.* 1997).

At the present time, because of the imprecise geochronology and uncertain biostratigraphy, the only means for advancing the concept of orbitally forced cyclochronology for the Jurassic Period is through identification of orbital signals in stratigraphy by use of two or more methods of analysis, such as those presented in this paper. Below, we discuss a South Alpine cyclic carbonate sequence spanning the Lower–Middle Jurassic boundary (figures 1 and 2), which reveals strong evidence for sustained orbital forcing. Some of the arguments leading to our conclusions are made without explicit reference to the available radiometric geochronology, which over the Pliensbachian–Bajocian interval is the least accurately constrained of the Jurassic Period (Gradstein *et al.* 1995). Instead, the considerable thickness (hundreds of metres) of the sequence and its nearly continuous stack of hundreds of thin bedded (cm–dm-scale) carbonate–shale cycles, allowed us to explore the orbital forcing hypothesis by examination of stratigraphic cycle thickness modulations and comparison with the long-term frequency modulation patterns of basic orbital signals. This frequency modulation approach does not require tuning of the data, or a precise



time-scale, although, as a final step, assessment of the results against an independent time-scale is necessary.

The cyclostratigraphic modulation spectra estimated from these Jurassic data compare closely with basic orbital modulation model spectra, and we regard this as compelling evidence for orbital control of the cycles. In the case of the Pliensbachian Domaro Limestone, this result led us to infer (net) accumulation rates for the limestone and shale couplet lithologies, reconstruction of an incremental time-scale, and direct recovery of a dual frequency signal closely resembling that of the precession. The FM modelling also allowed us, together with geological considerations concerning the origin of the cyclic carbonate deposition, to propose specific physical mechanisms that might have connected the orbital insolation driver to the depositional process. Finally, the most striking result of our analysis was the discovery of a fundamental switch in cycle mode from dominant forcing by the precession parameter in the Pliensbachian Domaro Limestone, to pure obliquity forcing in the overlying Toarcian–Aalenian Sogno Formation, with the switchover occurring some-



time during the deposition of the Lower Toarcian black shale. This modal switch was attended by other significant global changes, including major hydrologic shifts on land, widespread oceanic anoxia, and evidence for global cooling and subsequent eustatic drawdown.

We conclude with a proposed cyclochronology for the duration of the Toarcian–Aalenian Stages, and offer some predictions for the biozonation of the Pliensbachian Domaro Limestone, which at Colle di Sogno has an undefined lower biostratigraphic boundary.

## 2. Frequency modulation analysis of orbital signals

In the endeavour to develop spectrally based criteria to test the Milankovitch hypothesis in the absence of a precise time-scale, we turned to the concept of cycle modulation analysis. For some time, it has been proposed that the precession, as the globally dominant orbital parameter that forces insolation, might be connected with the carbonate productivity response of the surface ocean, leading to the formation of pelagic carbonate cyclic sequences. Thus, the primary amplitude modulation of the 21 ka precession carrier by the *ca.* 100 ka orbital eccentricity would explain the *ca.* 5:1 grouping, or ‘bundling’, of cycle thicknesses sometimes observed in these sequences (e.g. Schwarzacher & Fischer 1982). Herbert (1992) offered a slight but significant variation on this hypothesis, proposing that cycle thickness bundling could instead be linearly related to the frequency modulation of the precession, i.e. stratigraphic cycle thickness is proportional to precession cycle duration. In the field, the Colle di Sogno cycles indeed appeared to be bundled, but our data collection did not recover accurate representations of cycle amplitudes (e.g. by evaluation of per cent carbonate or some other geochemical or isotopic proxy), only cycle thickness defined by lithologic ‘ranks’. Therefore, we restricted our study to the frequency modulation hypothesis. We used the methods of Thomson (1982) for spectral analysis throughout the paper.

The procedure used in this study to estimate the frequency modulations of a stratigraphic signal corresponds to the ‘metronomic’ FM signal estimation of Herbert (1992, 1994). FM estimation is a robust analyser of the basic orbital signals that are expected to drive cyclic sedimentation. This robustness is illustrated by three simple case studies (figure 3) that embody the most serious problem in orbital signal recovery from cyclic sedimentary sequences, namely, variable accumulation rate.

Case 1 is a two-component stratigraphic signal accumulating at  $1 \text{ cm ka}^{-1}$  and recording simultaneously operating sinusoids of frequencies  $f_1 = 1/22.22 \text{ cm}^{-1}$  and  $f_2 = 1/18.18 \text{ cm}^{-1}$ , representing a simplified ‘precession’ (figure 3*a, b*). Metronomic FM analysis of this signal reveals that the thickness sequence of the stratigraphic cycles is itself cyclic (figure 3*c*), with a major FM peak labelled ‘a’ at  $f = 0.18$  cycles/unit (figure 3*d*), reflecting a 5.5 cycle ‘bundling’ period in the FM signal. That is, there is a repetition in cycle thicknesses that occurs approximately every 5.5 cycles. Other subsidiary FM peaks in figure 3*d* are overtones of ‘a’, and are the consequence of the highly distorted form of the FM signal. The peak in brackets indicates an overtone that actually occurs beyond the Nyquist frequency, but appears here as an alias. Case 2 is a one-component stratigraphic signal, a sinusoid of frequency  $f_1$ , accumulating initially at  $1 \text{ cm ka}^{-1}$ , which is then suddenly subjected to an accumulation rate decrease of 18.18% (figure 3*e*). The spectrum of this stratigraphic signal is identical to the Case 1 signal (figure 3*f*), because, with no *a priori*

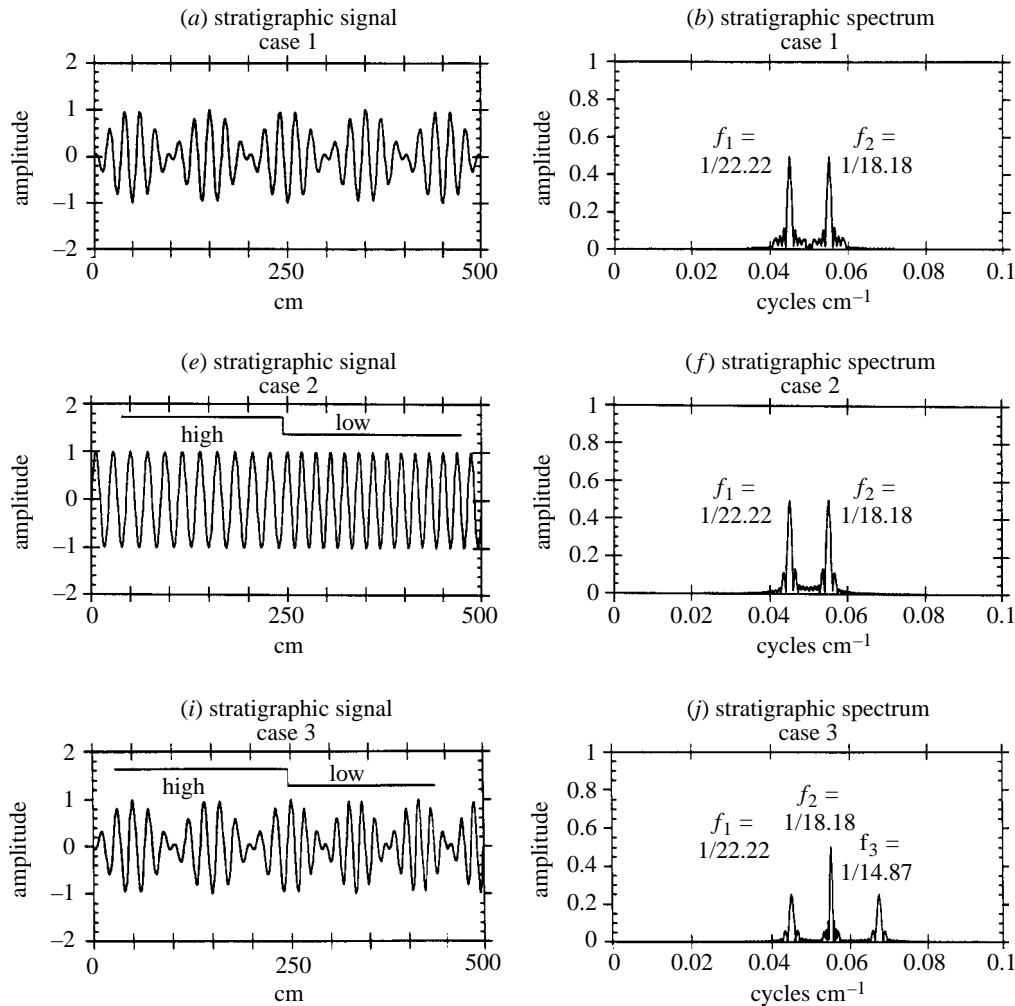


Figure 3. (a) Case 1 modulating stratigraphic signal composed of two simultaneously operating sinusoids of frequencies  $f_1 = 1/22.22 \text{ cm}^{-1}$  and  $f_2 = 1/18.18 \text{ cm}^{-1}$  accumulating at  $1 \text{ cm ka}^{-1}$ . (b) Spectrum of the Case 1 stratigraphic signal. (c) Metronomic FM signal of the Case 1 signal calculated over 20 m. Note the primary 'bundling' of cycle durations into groups of approximately (but not precisely) five. (d) Spectrum of the Case 1 metronomic FM signal, showing a primary FM component in the spectral peak 'a' at  $f = 0.18 \text{ cycles/unit}$ , reflecting 5.5:1 thickness bundling. Other higher frequency peaks are overtones of 'a'. Specifically,  $2^*a$  occurs at  $f = 2 \times 0.18 \text{ cycles/unit} = 0.36 \text{ cycles/unit}$ , and  $[3^*a]$  originating from the overtone  $f = 3 \times 0.18 \text{ cycles/unit} = 0.54 \text{ cycles/unit}$ , aliased into  $f_{\text{alias}} = 0.50 - (0.54 - 0.50) \text{ cycles/unit} = 0.46 \text{ cycles/unit}$ . (e) Case 2 modulated stratigraphic signal initially accumulating at  $1 \text{ cm ka}^{-1}$  with one frequency  $f_1 = 1/22.22 \text{ cm}^{-1}$  calculated over 20 m, but then subjected to an 18.18% accumulation rate decrease at 10 m. (f) Spectrum of the Case 2 stratigraphic signal.

information about the accumulation rate change, all of the frequency components detected along the entire length of the signal are projected onto the single-frequency scale of the spectrum. On the other hand, the FM signal (figure 3g) has an 'aperiodic' spectrum (figure 3h), with power near the zero frequency, reflecting the sudden accu-

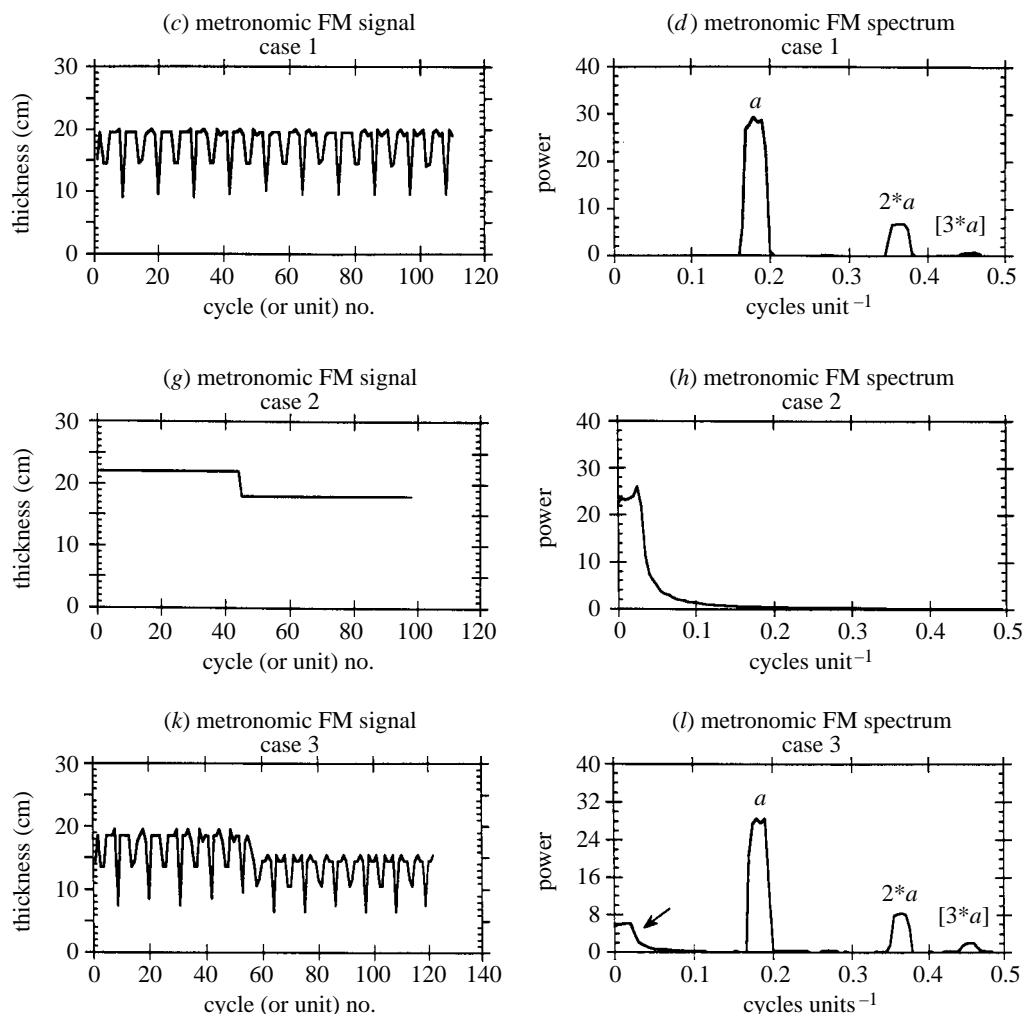


Figure 3. (*Cont.*) (*g*) Metronomic FM signal estimate of the Case 2 signal calculated over 20 m, with the 18.18% sedimentation rate decrease occurring at 10 m. (*h*) Spectrum of the Case 2 metronomic FM signal showing no bundling, but high power near the zero frequency. (*i*) Case 3, the Case 1 stratigraphic signal subjected to the sedimentation rate decrease of Case 2. (*j*) Spectrum of the Case 1 stratigraphic signal, showing three frequencies peaks as a result of the sedimentation rate change. (*k*) Metronomic FM signal estimate of Case 3 calculated over 20 m, with the 18.18% accumulation rate decrease occurring at 10 m. (*l*) Spectrum of the Case 3 metronomic FM signal, showing conservation of the FM spectral peaks Case 1, with the arrow indicating the near-zero frequency power contribution from the accumulation rate decrease.

mulation rate decrease, and the squeezing of the  $f_1$  cycle wavelength ( $1/22 \text{ cm}^{-1}$ ) to  $f_2$  ( $1/18.18 \text{ cm}^{-1}$ ) over the second half of the signal.

Of great significance is that the stratigraphic spectra of the original signals of Cases 1 and 2 (figure 3*b, f*) are not sufficient to ascribe a 'precession' origin to either signal. An interpretation of precession forcing would be correct for Case 1, but not for Case 2, where a single component of frequency  $f_1$  has been modulated by a step

function (18.18% decrease in accumulation rate) to a new frequency  $f_1/0.1818 = f_2$ . On the other hand, metronomic FM analysis of the signal easily distinguishes between Case 1 and Case 2. Finally, Case 3 is Case 1 subjected to the accumulation rate decrease of Case 2 (figure 3*i*). The spectrum of this stratigraphic signal (figure 3*j*) now exhibits three spectral peaks, at  $f_1$ ,  $f_2$ , and  $f_3 (= f_2/0.1818)$ . In fact, a total of four spectra are possible; in this case, the stepped accumulation rate modulator has piled  $f_1/0.1818$  onto  $f_2$  (note the doubled amplitude at  $f_2$ ) over the second half of the signal. It is no longer possible to determine the original component pair in the spectral analysis. However, metronomic FM analysis (figure 3*k, l*) fully retains the bundle peaks of Case 1 (compare with figure 3*c, d*); the accumulation rate modulation appears with low power near the zero frequency (see arrow), as in Case 2 (compare with figure 3*h*). This shows that metronomic FM analysis is resistant to accumulation rate changes that can produce otherwise profound changes in a conventional spectral analysis.

FM signal reconstructions of the precession and obliquity parameters are shown in figure 4*a, c*. There are numerous ways to construct FM signals; we elected to estimate durations between every other crossing of the signal over the signal's long-term mean, to mimic our FM signal reconstructions of the cyclic sequences. While the independent variable recorded here is uniformly sampled cycle number, the signals are actually non-uniformly sampled with respect to time. We applied the same procedure to our data, hypothesizing that the cycle thickness sequences comprising the FM signal estimates were similarly non-uniformly sampled in time. This representation is known as the 'metronomic' FM signal to emphasize the idea that the basic stratigraphic cycle is forced by a stable carrier frequency (Herbert 1992, 1994). The other representation, the 'stratigraphic' FM signal, records cycle thickness as a function of true stratigraphic position, an operation that unfortunately leaves open the possibility for signal distortion in the presence of long-term variations in accumulation rate, and causing significant defocusing of bundling frequencies (Herbert 1992). The 'metronomic' FM signal, on the other hand, remains unresponsive to long-term accumulation rate changes, instead recording such changes in the dependent (thickness) variable, which is then incorporated into thickness bundling power, *leaving bundling frequencies intact* (cf. figure 3). Finally, the main restriction of FM analysis in orbital studies is that, as a narrow band operator, the technique is not appropriate for the study of mixed precession–obliquity orbital signals; in addition, long datasets are required, preferably sequences with at least 100 cycles.

The quasi-periodicity of the orbital parameters is captured in the metronomic FM spectra of the precession index and obliquity (figure 4*b, d*). In the FM precession spectrum, the three peaks labelled  $\alpha$ ,  $\beta$  and  $\gamma$ , represent principal cycle duration 'bundling' frequencies; their origin is summarized in table 1. The  $\beta$  and  $\gamma$  components could reflect the expression of the approximately 1:5 bundling observed in various Mesozoic sequences; the bundling is actually bimodal, at 1:5.5 and 1:4.5, and is an expression of the dual-component (128 ka and 95 ka) 'short' eccentricity. In addition, an even more pronounced component  $\alpha$  is present, indicating a 'superbundling' component at 1:20; this derives from the high-amplitude, 404 ka 'long' eccentricity. The component labelled  $\delta$  was previously explained as another principal difference tone (Hinnov & Park 1998), but it is actually an overtone of  $\beta$ ,  $\delta'$  is an overtone of  $\gamma$ , and  $\delta^0$  an overtone of  $\alpha'$ . In contrast, the FM signal of the obliquity shows bundling components  $\varepsilon^0$ ,  $\varepsilon$ ,  $\varepsilon'$  and  $\varepsilon''$  (table 2). The dominant component  $\varepsilon$

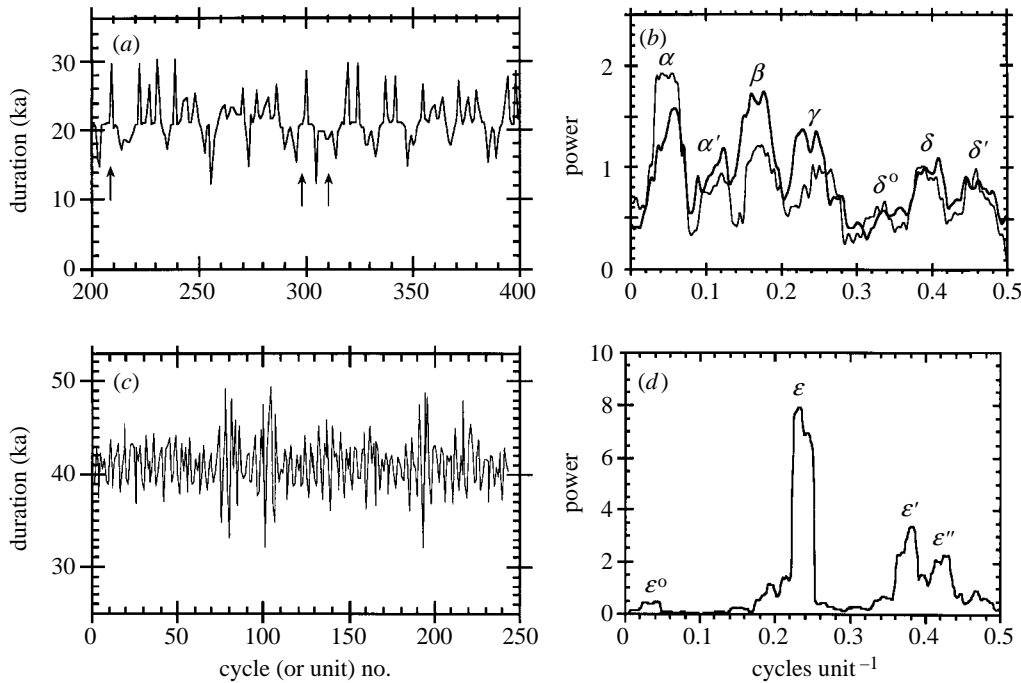


Figure 4. Basic FM orbital signal models. (a) FM signal of the precession calculated over the interval 16–12 Ma, a duration approximating the 160 cycle long Domaro cycle thickness sequence (compare with figure 5a). To obtain the precession signal, we used the FORTRAN program of Berger (1978), with updated tables from Berger *et al.* (1988). (b)  $4\pi$ -tapered power spectra of the FM precession over different 160 cycle long intervals, from 16 to 12 Ma and from 12 to 8 Ma, to highlight the stability of the peak frequencies. The origins of  $\alpha$ ,  $\beta$  and  $\gamma$  are outlined in table 1, and  $\alpha'$  is a transient 1:10 component that appears sporadically (see arrows in (a)). Note how the three highest frequency components  $\delta^0$ ,  $\delta$  and  $\delta'$  mimic the triplet  $\alpha'$ ,  $\beta$  and  $\gamma$ ; the former are in fact overtones of the latter. They do not occur at a precise integer multiple of the fundamentals because the FM signal itself has a greatly distorted shape with sharp, narrow peaks and rounded, wide troughs, which has the effect of reducing the frequency separation between fundamental and overtone. (c) FM signal of the obliquity calculated over 0–10 Ma, a duration like that of the Sogno cycle thickness cycles (compare with figure 6a). (d)  $4\pi$  power spectrum of the FM obliquity signal in (c), revealing FM frequencies at  $\varepsilon^0$ ,  $\varepsilon$ ,  $\varepsilon'$  and  $\varepsilon''$ , the origins of which are summarized in table 2.

has a cycle duration bundling of 1:4.25; actually  $\varepsilon$  incorporates a second lower power component with bundling at 1:3.74.

The FM approach used here is empirical in nature, designed to test the hypothesis that stratigraphic cycle thickness modulations are related to orbital cycle duration modulations. The modulating signals, both in the stratigraphic data and in the orbital theory, are treated as having high-frequency ‘carriers’ modulated by low-frequency ‘modulators.’ Since the data and the theory are to be connected in this way, then we must understand the sources underlying the modulating theoretical orbital signals.

For the precession index, the connection between ‘carrier’ and ‘modulator’ is embodied in the expression  $e \sin \omega t$ , where  $e = e(t)$  is the orbital eccentricity (the

Table 1. *Metronomic frequency modulation tones of the precession index*

((a) FM components for today's precession index, using frequency components  $1/23.72 \text{ ka}^{-1}$ ,  $1/22.43 \text{ ka}^{-1}$ ,  $1/18.98 \text{ ka}^{-1}$  estimated using the formula  $k + g_i$  as described in Berger *et al.* (1992), with  $k = 50.417262'' \text{ a}^{-1}$ , and the fundamental frequencies  $g_5$ ,  $g_2$  and  $g_4$ , respectively, from Laskar (1990, table VIII). (b) FM components estimated for a theoretical Middle Jurassic precession index, with  $k = 53.80204918'' \text{ a}^{-1}$  interpolated from the evolution of  $k$  in Berger & Loutre (1994), and  $g_i$  taken from 175 Ma in fig. 8 of Laskar (1990), to yield frequency components  $1/22.33 \text{ ka}^{-1}$ ,  $1/21.16 \text{ ka}^{-1}$ , and  $1/18.07 \text{ ka}^{-1}$ .)

(a) today		
FM component	difference tone ( $\text{ka}^{-1}$ )	FM tone (cycles/unit)
$\alpha$	$1/22.39 - 1/23.71 = 1/402.2$	$21.0/402.2 = 0.052$
$\beta$	$1/18.96 - 1/22.39 = 1/123.8$	$21.0/123.8 = 0.170$
$\gamma$	$1/18.96 - 1/23.71 = 1/94.64$	$21.0/94.64 = 0.222$
(b) Middle Jurassic (175 Ma)		
FM component	difference tone ( $\text{ka}^{-1}$ )	FM tone (cycles/unit)
$\alpha$	$1/21.16 - 1/22.33 = 1/403.8$	$20.0/403.8 = 0.049$
$\beta$	$1/18.07 - 1/21.16 = 1/123.8$	$20.0/123.8 = 0.161$
$\gamma$	$1/18.07 - 1/22.33 = 1/94.72$	$20.0/94.72 = 0.211$

modulator), itself a quasi-periodic signal, and  $\sin \omega t$ , the high-frequency carrier, describes the moving longitude of perihelion. Climate changes tracking the precession index are related to the timing of the Earth's seasons relative to the changing Earth-Sun distance at different points on its elliptical orbit. All else being equal, a Northern Hemisphere summer that occurs at perihelion (closest approach to the Sun) will be warmer than one that occurs at aphelion (greatest distance from the Sun). The moving longitude of perihelion acts to shift the timing of Earth seasons around the elliptical orbit, leading to the primary cyclic signal. Variations in the eccentricity of the orbit modulate the strength of the seasonal changes, and so modulate the precessional climate cycle that comes to be recorded in strata. Technically, the carrier frequency  $\omega = k + \Pi$  is not strictly constant, because  $k$ , the precession constant, is subject to secular change in the Earth's rotation (see below), and  $\Pi$ , the general precession, experiences planetary perturbations. Over time spans up to 20 Ma typical of stratigraphic sequences, however,  $\omega$  can be assumed to be approximately stable with a constant period of variation, e.g. 21 ka for recent times.

On the other hand, a similar decomposition of the obliquity variation into 'carrier' and 'modulator' signals is not so straightforward. The obliquity variation suffers only weak modulation, appearing in astronomical series as nearly monochromatic, that is, primarily as a single spectral peak. Nevertheless, there are modulating influences that result from planetary perturbations acting on the precession constant  $k$  (Berger & Loutre 1990). These perturbations act with fundamental frequencies  $s_i$ , resulting in a suite of frequencies in the obliquity variation, the most prominent ones closely spaced at  $1/41 \text{ ka}^{-1}$ ,  $1/39 \text{ ka}^{-1}$ ,  $1/54 \text{ ka}^{-1}$ ,  $1/29 \text{ ka}^{-1}$  (Laskar, this issue, table 6). Thus, while the variation behaves as a carrier signal experiencing long-period modulations, there is no underlying physical 'carrier' of the obliquity variation (analogous to  $\sin \omega t$

Table 2. *Metronomic frequency modulation components of the obliquity*

((a) FM components for today's obliquity variation, using frequency components  $1/41 \text{ ka}^{-1}$ ,  $1/39.73 \text{ ka}^{-1}$ ,  $1/53.62 \text{ ka}^{-1}$ , and  $1/28.9 \text{ ka}^{-1}$ , estimated using the formula  $k + s_i$ , with  $k$  as in table 1a and the fundamental frequencies  $s_3$ ,  $s_4$ ,  $s_6$ , and  $s_1$ , respectively, from Laskar (1990, table VIII). (b) FM components estimated for a theoretical Middle Jurassic obliquity variation, with  $k = 53.80204918'' \text{ a}^{-1}$  as in table 1b, and  $s_i$  taken from 175 Ma in fig. 9 of Laskar (1990), to yield frequency components  $1/37.11 \text{ ka}^{-1}$ ,  $1/35.99 \text{ ka}^{-1}$ ,  $1/47.18 \text{ ka}^{-1}$ , and  $1/26.89 \text{ ka}^{-1}$ .)

(a) today		
FM component	difference tone ( $\text{ka}^{-1}$ )	FM tone (cycles/unit)
$\varepsilon^0$	$1/39.73 - 1/41.0 = 1/1282.6$	$41.0/1282.6 = 0.032$
$\varepsilon$	$1/41.0 - 1/53.62 = 1/174.2$	$41/174.20 = 0.235$
	$1/39.73 - 1/53.62 = 1/153.4$	$41/153.4 = 0.267$
$\varepsilon'$	$1/28.91 - 1/39.73 = 1/106.2$	$41/106.2 = 0.386$
$\varepsilon''$	$1/28.91 - 1/41.0 = 1/98.0$	$41/98.04 = 0.418$
(b) Middle Jurassic (175 Ma)		
FM component	difference tone ( $\text{ka}^{-1}$ )	FM tone (cycles/unit)
$\varepsilon^0$	$1/35.99 - 1/37.11 = 1/1192.5$	$37/1192.5 = 0.031$
$\varepsilon$	$1/37.11 - 1/47.18 = 1/173.9$	$37/173.9 = 0.213$
	$1/35.99 - 1/47.18 = 1/151.7$	$37/151.7 = 0.244$
$\varepsilon'$	$1/26.89 - 1/35.99 = 1/106.3$	$37/106.3 = 0.348$
$\varepsilon''$	$1/26.89 - 1/37.11 = 1/97.6$	$37/97.6 = 0.379$

of the precession index). Our FM treatment of the obliquity signal thus amounts to an analysis of the 'beat' frequencies of its major components.

The FM components of both the precession and obliquity are dependent on the behaviour of  $k$ , which in turn is dependent on the Earth's rotation rate (Berger *et al.* 1992). The Jurassic Period is predicted to have had a shorter length of day, which results in larger  $k$ ; this in turn shortens the effective frequencies of the precession index. Since eccentricity is thought to remain stable throughout the Phanerozoic (Laskar, this issue), a shorter Jurassic precession carrier will complete more cycles within the same principal periods of the eccentricity modulator, and the metronomic FM components in figure 4b will shift (slightly) to lower frequencies. If the planetary perturbations affecting the obliquity variation likewise remain stable, then the main contribution to the change in obliquity back in time will also be in  $k$ , the resulting frequencies of the variation will also shorten, and in the metronomic FM analysis, the FM obliquity components in figure 4d will also shift to lower frequencies. We provide predictions for these shifts for early Middle Jurassic times (175 Ma) for the metronomic FM components of the precession and obliquity in tables 1 and 2.

### 3. The Pliensbachian Domaro Limestone

The Domaro Limestone is the youngest member of the Liassic Moltrasio Group, a thick basinal carbonate sequence in the Lombardy Pre-Alps of northern Italy (Montanari 1974; Gaetani 1975) (figures 2 and 5). At Colle di Sogno, the Domaro is

characterized by a *ca.* 35 m lower interval of hundreds of remarkably uniform cycles composed of dm-scale siliceous limestones interbedded with cm-scale, highly compacted shales. The limestone is a biomicrite, with skeletal remains from pelagic and neritic organisms floating in a micritic matrix rich in calcitic peloids and microspar. One or two chert bands parallel to bedding occur in individual limestone beds; these are rich in sponge spicules. The sediment is well bioturbated with burrows parallel to subparallel to bedding. There is no evidence of compaction in the micrite except near the shale contacts where there are stylolites.

Understanding the source of micrite in basinal formations of this age has been an enduring problem in sedimentology (Kälin 1980). The two possibilities are platform-derived carbonate mud from nearby shelves, or pelagic (nannofossil) ooze. Quantitative study of micrites elsewhere from the Lombard Basin at sites proximal (Carpeneda) and distal (Monte Generoso) to the Venetian Platform (figure 1), 5 and 150 km away, respectively, indicate contributions of only a few per cent of nannofossils by volume to the total carbonate at Generoso, and an order of magnitude less at Carpeneda (Picotti & Cobianchi 1996). This suggests that the nannofossils are diluted by major contributions of platform carbonate mud into the basin, ten times more so at the Venetian toe-of-slope.

The highly compacted shaly interbeds contain abundant clays (illite), organic material, discontinuous marly lenses, and detrital feldspars and quartz. These latter two components were not observed in the micrites, suggesting that the shales represent erosive phases and a continental provenance.

This cyclic interval is overlain by another *ca.* 45 m interval of thicker, variable bedding containing significant and sometimes coarse neritic carbonate skeletal debris. Synsedimentary slumps reflect Late Pliensbachian tectonics (rifting) that affected the region (Winterer & Bosellini 1981; Sarti *et al.* 1992; Bertotti *et al.* 1993). The Pliensbachian–Toarcian boundary is marked by the appearance of *Dactyloceras* and a sudden change to red/marly arenaceous lithologies (the basal Sogno Formation, see next section).

The Domaro Limestone has been described to encompass the entire Domerian Substage (*stokesi-spinatum* zones) (e.g. Montanari 1974), but at Colle di Sogno, the start of the formation has not been located due to lack of biostratigraphy. We have placed the formation base provisionally at the horizon where cyclic bedding thicknesses decrease abruptly from those of the main Moltrasio Group limestones. However, depending on the origin and timing of the cycles, this horizon may lie in the Carixian Substage (*jamesoni-davoei* zones) (Hinnov & Park 1998; see also below). Radiometric geochronology from Gradstein *et al.* (1995) constrains the duration of the Domerian to  $2.34 \pm 0.37$  Ma, assuming an equal (Hettangian–Bajocian) ammonite subzone chron duration of  $0.468 \pm 0.073$  Ma. Thus, the average accumulation rate for the entire Domaro Limestone (as provisionally defined in figure 2) is of the order of  $4 \text{ cm ka}^{-1}$ , somewhat high for a basinal site (Enos 1991). The upper *ca.* 45 m, with its thick gravity deposits of neritic material, may have accumulated at rates much faster than this average, and the lower cyclic interval at much slower rates. It is also possible that the subzones have extremely variable durations within the Domerian (see Van Buchem *et al.* (1994) and Weedon & Jenkyns (1999) for estimates of individual Pliensbachian ammonite zone durations).

A limestone–shale couplet thickness sequence from the lower *ca.* 35 m of the formation is shown in figure 5a, and exhibits clear multicomponent 1:20 and *ca.* 1:5

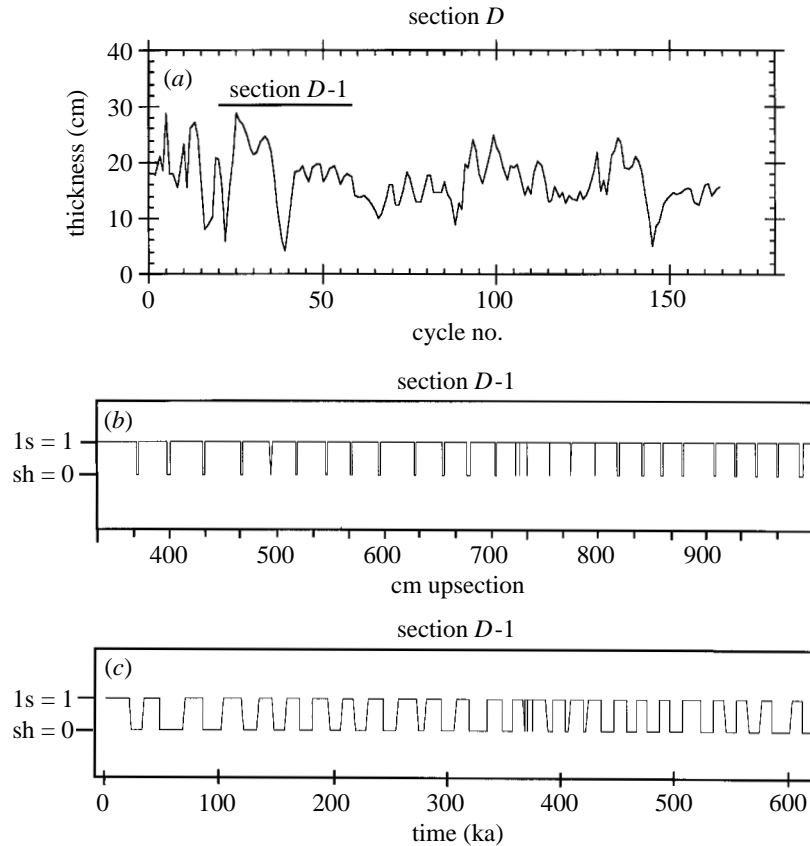


Figure 5. (a) The Domaro thickness sequence over cycle nos 1–160 (Section *D* in figure 2), smoothed by a three-point moving average. (b) Detail of the rank depth series, sampled at intervals  $\Delta d = 0.1$  mm, from metres 3.7 to 8.4 (Section *D-1*, see figures 2 and 5a). (c) Reconstructed rank time-series of Section *D-1* (figure 5b), sampled at  $\Delta t = 0.2$  ka intervals, from Hinnov & Park (1998).

thickness bundling. Figure 5b depicts a high-resolution rank series of the segment spanning cycle nos 24–54, and figure 5c shows the same segment converted to time. The power spectrum of the couplet thickness sequence is displayed in figure 6a and reveals major peaks recognizable as FM precession  $\alpha$ ,  $\beta$ ,  $\gamma$  and  $\delta$  components, suggesting that it is a high-resolution record of multicomponent precession. Hinnov & Park (1998) further analysed the limestone and shale thickness sequences separately (after Schwarzscher 1964) and concluded that the limestone and shale lithologies had been deposited during complementary times within precession cycles. This information was used to estimate the accumulation rates of the limestone and (compacted) shale lithologies at  $1.57 \text{ cm ka}^{-1}$  and  $0.14 \text{ cm ka}^{-1}$ , respectively. These rates were then applied to obtain the incremental time-scale for the rank series in figure 5c. Thus, where the power spectrum of the rank depth series in figure 6b is extremely variable, with no dominating peaks, application of these accumulation rates focuses rank series power into a tightly defined dual frequency signal closely resembling that of a ‘clipped’ precession signal of similar length (figure 6c).

#### 4. The Toarcian–Aalenian Sogno Formation

The cyclic sedimentation of the Sogno Formation at Colle di Sogno (figures 2 and 7) is much different from that of the underlying Domaro Limestone, with 20–50 cm thick buff-coloured marly carbonates grading into and out of *ca.* 10 cm thick shaly marl interbeds. The formation is largely a *Posidonia alpina* facies, missing the spiculitic silica of the underlying Domaro, but gaining an abundance of the marker fossil *Bositra buchi*, and higher in the section, an increasing fraction of radiolarian chert. Commonly, individual limestone beds contain several continuous marly seams or thin shales parallel to bedding. In the field we recognized eight lithologies that occurred consistently throughout the formation, basically related to the biogenic carbonate/non-carbonate ratio. We measured the thicknesses of these lithologies to the nearest millimetre along the section, assigning a rank (1–8) for each lithology (figure 7). The appearance of a second biogenic component (radiolarian chert) was given the highest value of 8, and so the ranking is actually a measure of biogenic content.

The lowermost 4 m of the formation (figure 2) are characterized by a cyclic carbonate/marl interval mixed with poorly sorted terrigenous sediment (Gaetani & Poliani 1978). The next 4 m are marked by a gradual decrease in carbonate and replacement by thickening organic rich shales, although a regular cycle thickness of *ca.* 30 cm is maintained. Metres 8–16 are occupied by the Lower Toarcian black shale, the local expression of a global Oceanic Anoxic Event (Jenkyns 1988) and major transgression (Haq *et al.* 1988; see figure 11 below). The black shale is composed of organic rich, thinly laminated, pyritic shales that contain the remains of fish, crustacea, cephalopods, and land plants (Tintori 1977). Unfortunately, at Colle di Sogno the unit is mostly covered by the road, and so the record of any lithologic cyclicity within this most important interval cannot be recovered. At metre 16, the carbonate cycles resume as a true *Posidonia alpina* facies, with thick (0.5 m and greater) marly limestone/marl alternations, containing sometimes copious deposits of *Bositra buchi*; the presence of *Chondrites* indicates continued dysaerobia at the seabottom. Occasional thin (cm-scale) graded beds within cycles (indicative of limited redeposition events from local highs) also occur. The cycles thin gradually upsection, gaining a significant component of radiolarian chert during the Aalenian. *Zoophycos* also appears before the section terminates in the Lower Bajocian; the formation is overlain by the famous ribbon Radiolarites (Baumgartner 1987). As with the underlying Domaro, the origin of the Sogno's micritic carbonate most probably continues to be lime mud swept off platform areas (Picotti & Cobianchi 1996).

Sogno Formation biostratigraphy (figure 2) is based on ammonites for the Lower Toarcian, and on nannofossil stratigraphy for the remainder of the section. The most recent chronology by Gradstein *et al.* (1995) gives a duration of  $13.1 \pm 2.8$  Ma for the Toarcian–Aalenian interval, or an average sedimentation rate of  $9.92 \pm 2.12$  m Ma<sup>-1</sup>. The duration of the depositional gap between the Lower Bajocian and the overlying ribbon Radiolarites is thought to last until the Early Bathonian. These carbonate-free Radiolarites span the Bathonian–Oxfordian, a time during which no appreciable carbonate was deposited in most of the Lombard Basin. This curious, sustained absence of carbonate in the basin is thought to be related to collapse of the Venetian Platform (e.g. Zempolich 1993).

The Sogno cycle thickness sequence in figure 7a was obtained for metres 16–130 only, because in the pre-black shale interval the number of cycles (30) is too small

Table 3. *Estimated periods of the metronomic FM obliquity compared with the metronomic FM components of the Sogno Formation cycles*

(The FM obliquity component periods were estimated by computing the difference tones of the obliquity frequencies (as in table 2), and taking the inverse. The FM component periods of the Sogno cycles were computed by dividing the frequency components in figure 8a, i.e.  $\varepsilon^0 = 0.05$  cycles/unit,  $\varepsilon = 0.25$  cycles/unit,  $\varepsilon' = 0.47$  cycles/unit and  $\varepsilon'' = 0.53$  cycles/unit (this last component is inferred as appearing concurrently with  $\varepsilon'$  as an alias at  $f_{\text{alias}} = 0.47$  cycles/unit, and so is recorded in brackets) into 37 ka, the principal obliquity component period estimated for the Middle Jurassic (table 2b).)

	theoretical Jurassic obliquity metronomic FM cycle periods (ka)	Sogno Formation metronomic FM cycle periods (ka)
$\varepsilon^0$	1192.5	740
$\varepsilon$	173.9	148
$\varepsilon'$	106.3	79
$\varepsilon''$	97.6	[70]

to evaluate by the FM method. Lowpass filtering was applied to the rank series before cycle thickness estimation to avoid selecting ‘cycle’ thicknesses defined by the occasional mm-scale shaly seams that occur within the larger limestone/marl cycling members. Details of the raw rank depth series over key intervals in the section are shown in figure 7b–e.

The power spectrum of the cycle thickness sequence in figure 8a has major bundling components at frequencies with a spacing similar to those of the FM obliquity spectrum (compare with figure 4d), except that the peaks are systematically shifted to higher frequencies. Table 3 compares the periods (in ka) of the estimated metronomic FM components of the obliquity versus the Sogno cycles. All of the Sogno FM components show substantial period shortening. It is unclear if  $\varepsilon''$  is actually present in the aliased form as inferred (see caption to table 3). Possibly, intermittent hiatuses occur within the sequence as a result of an increased incidence of ‘missed beats’ during lower-amplitude sea-level oscillations, systematically producing slightly fewer sedimentary cycles per thickness bundle. The ‘missed beats’ phenomenon would have to occur in platform areas (the Venetian Platform, see figure 1) where carbonate productivity is no longer responding to lower-amplitude precession-driven sea-level oscillations. In this case, the Venetian Platform during Toarcian–Aalenian times first experienced a productivity crisis (eutrophication), followed by collapse and final demise during Bajocian times. Possibly these events are related in some way to these metronomic ‘anomalies’ in the platform-derived Sogno cycles.

An evolutionary spectral analysis of the entire Sogno rank depth series appears in Hinnov *et al.* (1999). Here, we summarize the main results of that analysis. From metres 0–4, there is no consistent cyclicity in the sequence; this can be explained by the disruption of the carbonate cycles by a substantial terrigenous influx, which apparently was not phased with the carbonate. On the other hand, the power spectrum for metres 4–8 in figure 8b reveals major components with frequency spacings consistent with short eccentricity and precession, and a third component at 9.5 ka when we tuned the lowest peak of the spectrum to 100 ka. Together these components could reflect a real change in the climatic-sedimentation response to precession

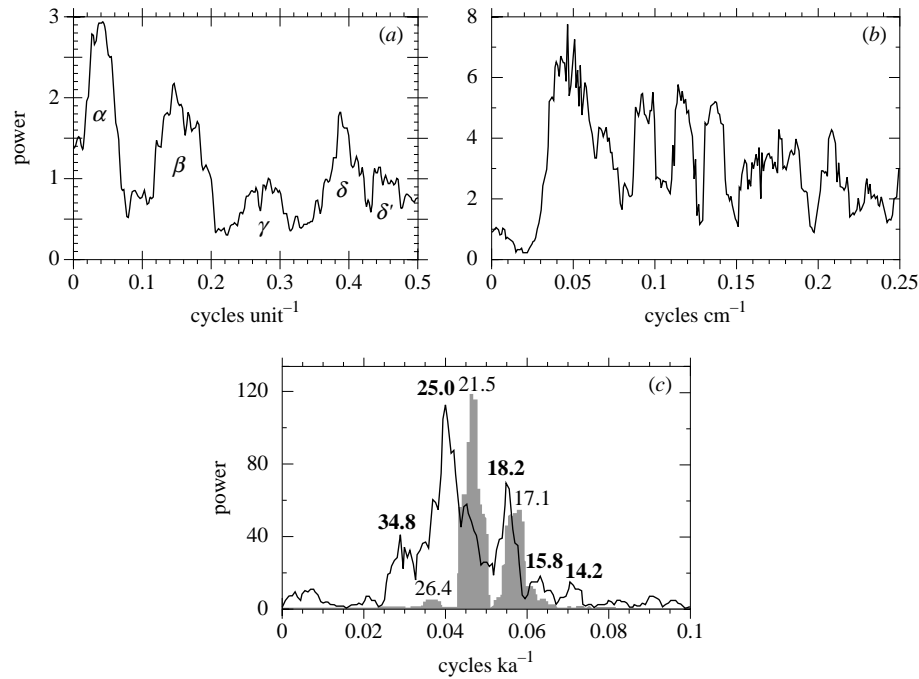


Figure 6. Spectral analysis of the Domaro Limestone. (a)  $4\pi$  power spectrum of the Domaro thickness sequence (Section *D*, see figure 5a), with peaks interpreted as FM precession components. In this case, the components labelled  $\delta$  and  $\delta'$  both appear to be related to the  $\beta$  component, which shows signs of splitting at  $f = 0.15$  cycles/unit and  $f = 0.18$  cycles/unit (see also fig. 15 in Hinnov & Park 1998). The  $\gamma$  component, at  $f = 0.28$  cycles/unit, also shows signs of splitting, but the overtone for this component, which would occur at  $f = 0.735$  cycles/unit (aliasing into 0.265 cycles/unit), could also be influencing this component. Splitting could be due to a hiatus in the sequence. (b)  $4\pi$  power spectrum of the Section *D-1* over cycle nos 24–54 (figure 5b), showing a multitude of peaks. Spectral analysis of series with two ranks such as this one is little improvement from a simple cycle thickness histogram. Here, cycle wavelengths cluster in a wide band centred near  $f = 0.05$  cycles  $\text{cm}^{-1}$  (ca. 20 cm cycle thicknesses, which is the average cycle thickness over this interval). Other higher-frequency peaks may be the result of the highly distorted (compacted shale) shapes of the rank cycles, i.e. they may be overtones or intermodulation tones if there is more than one frequency component present in the series. (c)  $2\pi$  power spectrum of the Section *D-1* transformed into a time-series using the accumulation rates of 1.57  $\text{cm ka}^{-1}$  and 0.14  $\text{cm ka}^{-1}$  for the limestone and shale ranked intervals, respectively, based on a somewhat high Jurassic precession carrier frequency of 1/19.4  $\text{ka}^{-1}$  (for full details see Hinnov & Park 1998). Power of the Domaro has collapsed into two bands at 1/25  $\text{ka}^{-1}$  and 1/18.2  $\text{ka}^{-1}$  (bold text labels, in period ka); these compare well in amplitude with the power spectrum of a 30-cycle long, 'clipped' Jurassic precession signal (shaded), with components at 1/21.5  $\text{ka}^{-1}$  and 1/17.1  $\text{ka}^{-1}$  (normal text labels, in period ka). These components are shorter than those computed in table 1 owing to other input parameters to the Berger (1978) FORTRAN program used to calculate the signal (see Hinnov & Park 1998, fig. 14 caption). The precession signal was clipped by assigning the value of 0 to precession values less than the long-term mean, and the value of 1 to values equal or greater than the mean. The other Domaro components at 1/34.8  $\text{ka}^{-1}$ , 1/15.8  $\text{ka}^{-1}$  and 1/14.2  $\text{ka}^{-1}$  are probably the results of small hiatuses and/or random perturbations in accumulation, although the ca. 1/34.8  $\text{ka}^{-1}$  component could be evidence of low-power obliquity (which has a predicted Jurassic frequency of 1/37  $\text{ka}^{-1}$ , cf. table 2b).

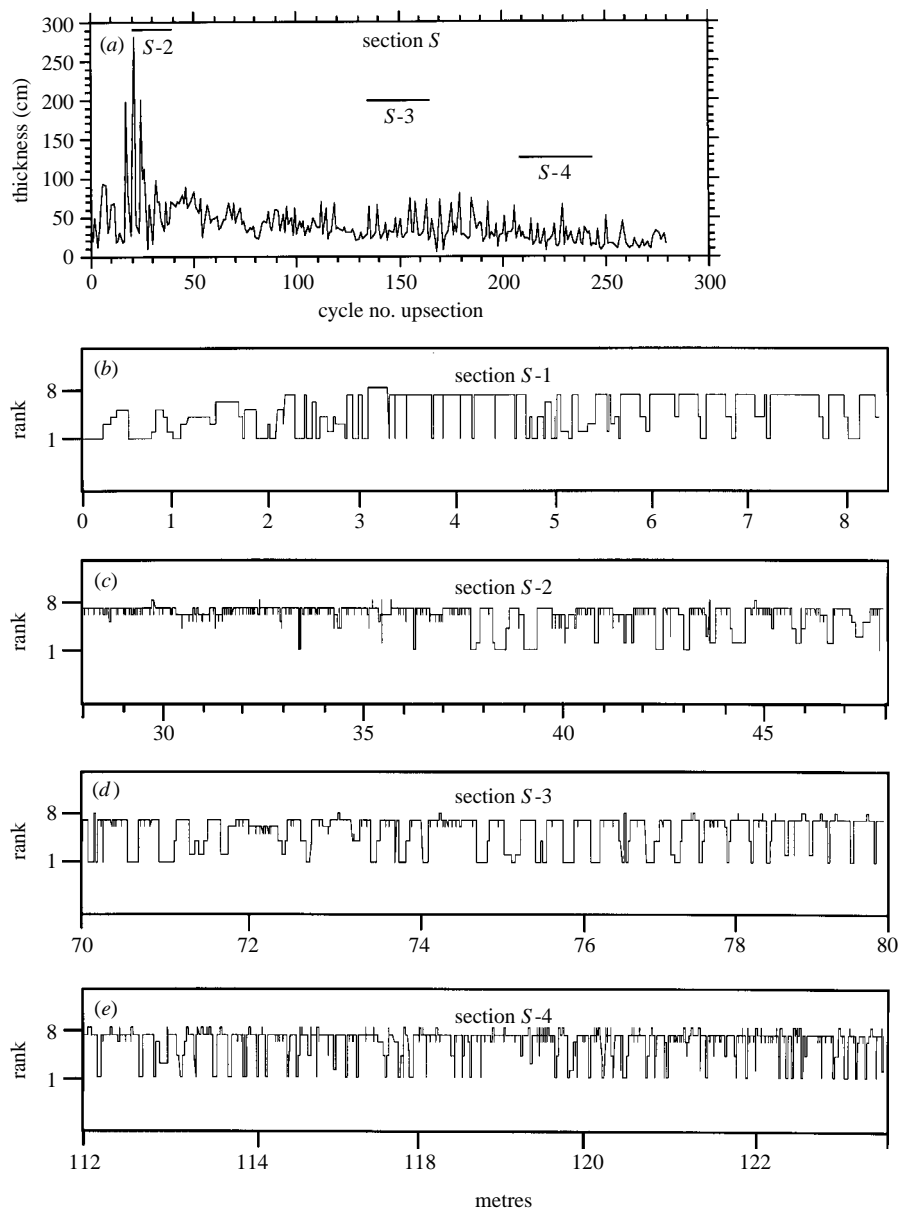


Figure 7. (a) The Sogno cycle thickness sequence over metres 16–140 (Section *S* in figure 2). The positions of the rank series *S-2*, *S-3* and *S-4*, plotted below, are indicated. Ranks are as follows: 1, shale; 2, marly shale; 3, shaly marl; 4, marl; 5, limey marl; 6, marly limestone; 7, limestone; 8, cherty limestone. (b) Section *S-1* from the pre-black shale interval. (c) The upper half of Section *S-2* from above the black shale, showing the termination of the high sedimentation interval at metre 37. (d) Section *S-3* from the Upper Toarcian; and (e) Section *S-4*, from the chert-rich Lithozone 3 in the Aalenian. The rank series was sampled at 0.1 mm for the entire formation. An evolutionary spectrum of the entire uninterrupted rank depth series from metres 16 to 130 appears in Hinnov *et al.* (1999).

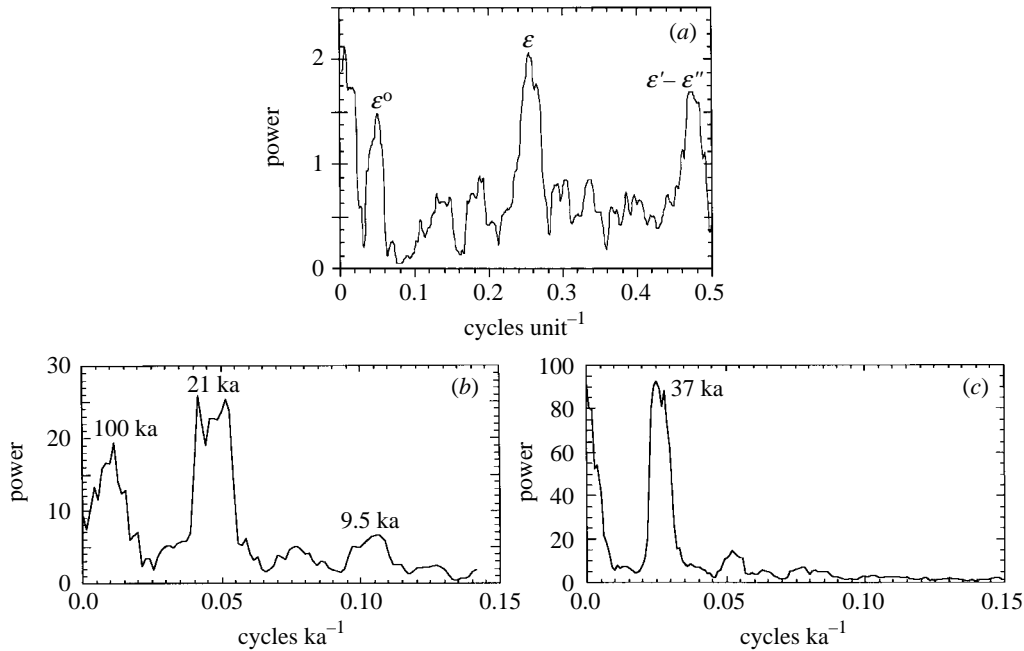


Figure 8. Spectral analysis of the Sogno Formation. (a)  $4\pi$  power spectrum of the Sogno thickness sequence (Section *S*, see figure 7a), over cycle nos 25–278, with peaks interpreted as FM obliquity components. (b)  $2\pi$  power spectrum of metres 4–8 (see Section *S*-1, figure 6b) in the pre-black shale portion of the formation. The lowest frequency component was tuned to a 100 ka period, yielding period estimates of 21 ka and 9.5 ka for the other two major components. The 21 ka component appears to be split, and harmonic analysis indicates that several lines make up this band, with periods at 21.9 ka (94% s.l.), 21.2 ka (99% s.l.), 20.5 ka (92.5% s.l.), and 17.5 ka (84% s.l.), where s.l. is significance level. For comparison, harmonic lines of a (noiseless) 4 Ma long Jurassic precession signal with input parameters as in figure 6, occur with periods at 21.5 ka (99.99% s.l.), 20.4 ka (99.99% s.l.) and 17.6 ka (99.5% s.l., slightly lower). (c)  $4\pi$  power spectrum of the post-black-shale interval from metres 16 to 42 (Section *S*-2, figure 7c), tuned to a 37 ka Jurassic obliquity period (see text for details). The smaller component at  $f = 0.055 \text{ ka}^{-1}$ , while within the Jurassic precession band, is actually the first overtone of the 37 ka component, shifted slightly to a lower frequency as a result of consistently thinner shales within the cycles.

(sensu Crowley *et al.* 1992) or could be artefacts of the rank depth series itself due to a systematically squeezed/stretched incremental time-scale within cycles from differing accumulation rates of the various ranked lithologies. Finally, figure 8c is a power spectrum from metres 16 to 43, showing a single-component signal consistent with obliquity. In fact, this component varies in frequency slowly and non-uniformly upsection, consistent with third-order eustatic variations (cf. Hinnov *et al.* 1999); for this spectral display we linearized this peak at 25 cm intervals using an evolutionary harmonic analysis over 2 m windows as a guide. The uni-modal aspect of this spectrum is characteristic of the entire post-black shale Sogno Formation, although decreasing accumulation rates, the thinning of the shalier lithologies relative to the carbonate beds, and the insertion of radiolarian chert upsection modify the wavelength of the signal, as well as the relative power and frequencies of over- and undertones.

While table 3 brings into question our interpretation of the Sogno cycles as obliq-

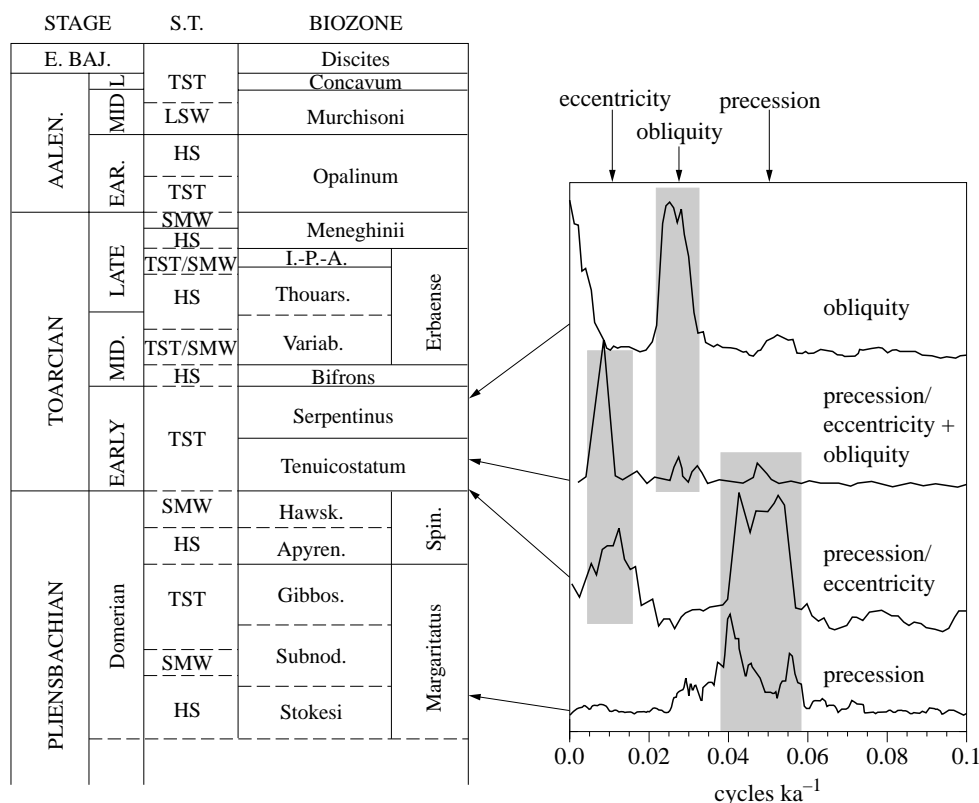


Figure 9. The evolution of orbital forcing in the carbonate cycles at Colle di Sogno, showing (1) dominant precession forcing in the Upper Pliensbachian, (2) the development of a multiple system (i.e. intraseasonal and/or interhemispheric) response to the precession in the lowermost Lower Toarcian, (3) a mixed precession/eccentricity and obliquity signal from the Lower Toarcian black shale in the east-lying Belluno Trough (Claps *et al.* 1995), and (4) pure obliquity forcing of carbonate in the post-black-shale interval. The lower Domaro cyclic interval may extend back into the Early Pliensbachian (Carixian), as explained in the text. S.T. are the sequence tracts of Haq *et al.* (1988).

uity driven, provided that the fundamental frequencies  $s_i$  in Laskar (1990) and estimates for Jurassic  $k$  in Berger & Loutre (1994) are reasonably accurate, we note nonetheless that the strong monochromatic cycle pattern throughout the post-black shale Sogno Formation is strongly suggestive of obliquity, as are the radiometric timing constraints on the cycles ( $41 \pm 31$  ka per Sogno cycle, i.e. the average Sogno cycle thickness is  $0.407 \pm 0.293$  m, and so  $0.407 \pm 0.293$  m /  $(9.92 \pm 2.12$  m Ma $^{-1}) = 0.041 \pm 0.0308$  Ma =  $41.0 \pm 30.8$  ka). This evidence, plus the mixed obliquity–precession patterns that occur in the black shale in the lower part of the formation, all point to obliquity as the primary driver of the Sogno cycles.

### 5. A precession to obliquity switch and associated global changes

In summary (figure 9), the Colle di Sogno sequence shows a long-term evolution of orbitally forced marine sedimentation with Late Pliensbachian dominant precession

forcing, followed by an altered precession response during the earliest Early Toarcian, and finally, a switch to pure obliquity forcing after deposition of the Lower Toarcian black shale. This points to the black shale as the interval in which the transition occurs, but unfortunately, at Colle di Sogno the shale is not accessible for sampling. However, Claps *et al.* (1995) examined an equivalent unit some 150 km to the east in the Belluno Trough (figure 1), and concluded that the carbonate thicknesses contained a mixed precession–obliquity signal (see figure 9). In addition to the presence of obliquity, the strong eccentricity component in the spectrum suggests a low latitude intraseasonal (as in Crowley *et al.* 1992) or interhemispheric (as proposed above for the pre-black shale interval) response to the precession.

In the nearby Monte Generoso Trough (figure 1), Weedon (1989) noted an evolution from multicomponent to single-component cyclicity in the Pliensbachian–Toarcian Morbio Formation and Ammonitico Rosso Lombardo, suggesting that the phenomenon at Colle di Sogno is not local. Also, descriptions of cyclic Toarcian basinal carbonates in the Spanish Subbetic Basin indicate a major shift in cycle mode during the Lower-Middle Toarcian. At Fuente de la Vidriera, a remarkably high-resolution section of this interval (nearly 100 m thick over the *polymorphum-gradata* [*tenuicostatum-variabilis*] subzones) shows a near doubling of cycle thicknesses from the *serpentinus* to the *bifrons* subzone (Jimenez *et al.* 1996); Upper Toarcian–Aalenian basinal cycle sequences in the Iberian Range are predominantly *ca.* 1:4-bundled in thickness (Gomez & Goy 1999; Goy *et al.* 1999). These patterns are suggestive of the bundling periods observed in the Sogno Formation, although a rigorous spectral analysis has not confirmed this.

An explanation for this Early Toarcian modal change in cyclic sedimentation response from precession to obliquity forcing in this tropical marine basin must begin with a discussion of the origin of the (micritic) carbonate and its relationship to orbitally forced insolation. The lack of evidence for significant ‘rock-producing’ nannofossil ooze during Early and Middle Jurassic times forces us to look to carbonate mud production in platform environments and transport into the basins as the likely source. Presumably, the mud would have been transported from the platform(s) in nepheloid suspension, and settled out onto the basin floor (in which case the Domaro and Sogno are technically hemipelagites). Carbonate production on platforms is governed by many variables, a principal one however being sea-level: whenever sea-level drops below the platform top, the carbonate factory shuts down or becomes restricted to shallow, narrow areas on margin slopes. In fact, the Liassic Venetian platform interior (figure 1) is composed of many hundreds of metre-scale subtidal carbonate cycles, many of which have thickness spectra with elements similar to the Domaro thickness spectrum, and that have been interpreted as the response of high-frequency sea-level oscillations (Claps 1993; Masetti *et al.* 1996). A similar thickness spectrum has also been reported in the Pliensbachian South Saharan Platform carbonate cycles of the High Atlas (Morocco), where palaeogradient estimates indicate sea-level changes of the order of 1–5 m (Crevello 1991). This evidence, along with orbital modelling of Hinnov & Park (1998) suggests that Domaro carbonate deposition was restricted to times of decreasing or low northern spring equatorial insolation (and thus increasing or high middle-latitude insolation). This points to platform lime mud production during sea-level rises or highstands, and platform shutdown and cessation of mud production during sea-level falls or lowstands. Also the presence of detrital feldspar and quartz in the Domaro shales suggests that the

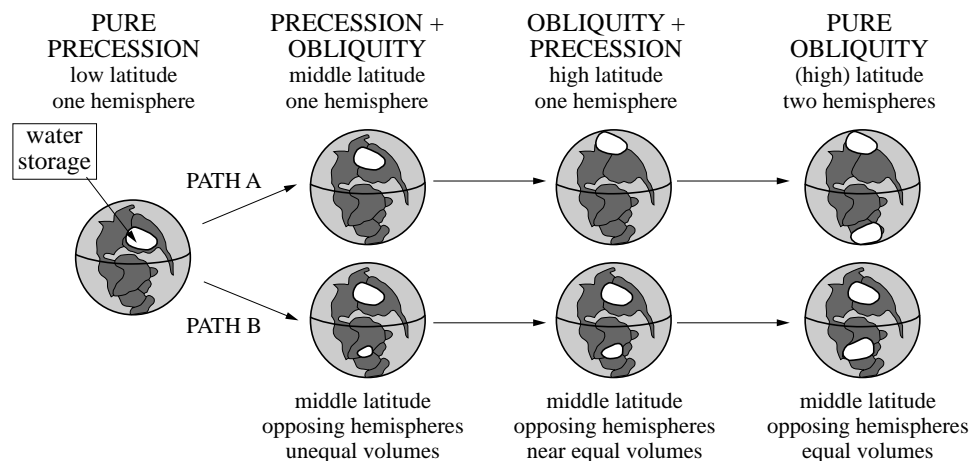


Figure 10. Proposed evolution of water (ice?) storage on continents that could explain the frequency evolution of the Colle di Sogno cycles as summarized in figure 9. We propose first that water sequestration on the continents is controlled by the local orbitally forced insolation, and second, that high-frequency eustasy is the sum of variations in the total continental water budget. Thus, to produce the frequency evolution of the Colle di Sogno cycles, zonal shifts in and the development of significant water reservoirs on the continents of both the Northern and Southern Hemispheres is required in order to suppress the precession in the eustasy, and to enhance the obliquity. The pathways that are sketched here (Paths A and B) are only two of an infinite number of possibilities, and it will remain impossible to decide on a specific solution without the collection of new data that covers the actual transition in the black shale interval, for advanced study of component phase for additional clues.

latter were deposited during marine regressive phases (lower base levels and increased continental erosion).

The climatic mechanism behind these proposed precession-driven Pliensbachian sea-level oscillations could involve some aspect, or all, of the following: (a) small orbitally driven mountain glaciers in middle latitude continental areas (Fischer & Hinnov 1997); (b) changes in water storage in middle latitude continental interiors (Jacobs & Sahagian 1995); or (c) thermal expansion of the oceans (Wigley & Raper 1987). The dominance of precession forcing in the Domaro Limestone tends to rule out ocean thermal expansion. This is because precession forcing is counterphased between the Northern and Southern Hemispheres, and so net sea-level oscillations in a global ocean from thermal expansion responses to the precession would be effectively zero. On the other hand, since obliquity-forced insolation is in phase between the hemispheres, we would expect a pure obliquity signal to characterize such thermally induced sea-level oscillations, which we do not see in the Domaro. Therefore, we favour a hypothesis involving orbitally controlled water sequestration on the continents to produce the sea-level oscillations. The absence of a significant obliquity component in the Domaro Limestone implies that during the Pliensbachian, orbitally forced water (ice?) storage was restricted to the low middle latitudes of a continent in either the Northern or Southern Hemisphere, i.e. latitudes with dominant precession forced insolation (figure 10).

The proposed obliquity-driven Sogno Formation presents a different situation, but

we offer a similar explanation. In this case, the problem is now to explain how the obliquity, nominally the major forcing parameter of polar climates, came to control basinal carbonate sedimentation in a tropical sea. Again, the answer can be explained as the result sea-level oscillations responding to a global shift in continental water storage (figure 10): either the effective global water storage moved poleward in one hemisphere (figure 10, Path A), or water storage began to increase at an opposing latitude in the other hemisphere (figure 10, Path B). We favour the latter possibility, since just before the appearance of obliquity, from metres 4 to 8 in the Sogno (figure 8*b*), there is evidence for a new, interfering response to precession in the global water storage (sea-level oscillations), suggestive of the introduction of an opposing, but unequal precession response from the other hemisphere. Finally, the development of pure obliquity-driven sea-level oscillations to control the production and exportation of platform mud into the basin would require bipolar, high-latitude orbitally forced water (ice) storage. This pattern is reminiscent of the pure obliquity variations in global sea-levels during the Pliocene, which could have arisen as a result of the growth of significant ice sheets in the Northern Hemisphere (Fischer & Hinnov 1997). This evolving change in effective orbital frequency was probably the result of the interhemispheric counterphasing precession components becoming suppressed in the integrated sea-level variations as northern ice sheets approached the size of those in Antarctica, at the same time reinforcing the obliquity component, which is in phase between the Northern and Southern Hemispheres.

Evidence for global changes that could account for a Toarcian precession to obliquity switch is summarized in figure 11. In Laurasia, there is palynological evidence for the development of humid conditions in Laurasia during the Toarcian (Vakhrameev 1991), indicating significant changes in the hydrology of at least one continent. In the western Tethyan basinal sections, the influx of kaolinite during the Toarcian from the west is consistent with increased humidity (Deconinck & Bernoulli 1991; Delavenna *et al.* 1989). There are also reports of glacial deposits from the Aalenian of Siberia (Frakes *et al.* 1992), and a disputed report of evidence for ice in Toarcian Antarctica (for details see Hallam 1975). A recent compilation of marine stable isotope data for the Toarcian–Bajocian interval by Podlaha *et al.* (1998) shows that  $\delta^{18}\text{O}$  values increased *ca.* 4‰ soon after the Early Toarcian oceanic anoxic event (OAE), the result of either decreasing marine temperatures, or increased removal of  $^{16}\text{O}$  from the oceans, or a combination of the two processes. Jenkyns & Clayton (1997) suggest that the increased biological productivity that characterized the oceans during the later phases of the Toarcian OAE could have shifted atmospheric  $\text{CO}_2$  to the oceans, resulting in global cooling during the Late Toarcian. The  $\delta^{18}\text{O}$  maximum coincides with sequence stratigraphic evidence (Haq *et al.* 1988) for the largest marine regression of the Jurassic (increase in landlocked water/ice?). Finally, climate modelling by Valdes *et al.* (1995) and Valdes & Glover (this issue) supports the possibility that there could have been significant seasonal snow at the poles during the Late Jurassic. Adjusting the model's atmospheric  $\text{CO}_2$ , and/or using the somewhat different continental distribution of the late Early Jurassic, might turn this into perennial ice.

## 6. Assessing the cyclochronology

Lack of knowledge of the biozonation of the cyclic interval in the Domaro Limestone, and the strong case for Domaro couplet forcing by the precession, presents an

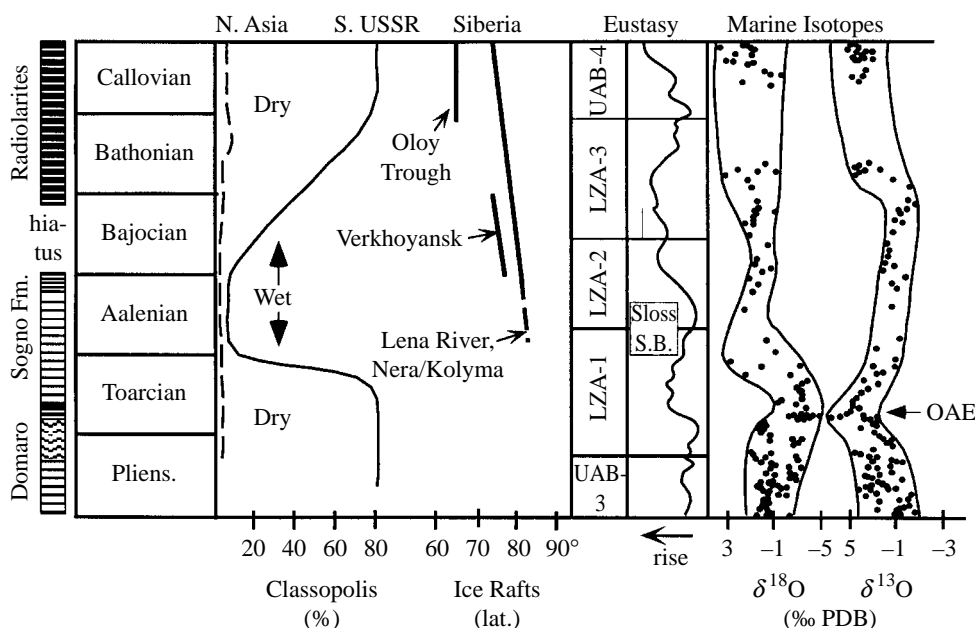


Figure 11. Summary of global changes during the Early–Middle Jurassic transition. On the far left is the Colle di Sogno section, with the Toarcian–Aalenian Sogno Formation that spans the ‘cooling event’ at the transition and ends in a basin-wide hiatus. Russian stratigraphic data tracks the abundance of the climate-sensitive palynomorph *Classopolis*, which disappears at the end of the Toarcian as a humid phase developed (Vakhrameev 1991). This lasted for all of the Aalenian at this location; a dry phase affected the remainder of the Middle Jurassic. Evidence of (episodic?) glaciation in northern Laurasia starts in the Aalenian with the appearance of dropstones in the stratigraphic record (Frakes *et al.* 1992). In addition, oxygen isotopes in belemnites shows that oceanic cooling occurred during this time (Podhala *et al.* 1998); also a major marine regression took place, resulting in the well known Early Aalenian Sloss (Type I) Sequence Boundary (Haq *et al.* 1988), which might also indicate the development of a significant volume of continental ice.

opportunity to discuss the duration of the interval. As mentioned earlier, the average ammonite subzone duration is  $0.468 \pm 0.073$  Ma. The Pliensbachian contains 15 ammonite subzones, which yields a duration of  $7.02 \pm 0.02$  Ma, which is within the uncertainties of durations obtained by radiometrically determined boundary ages, e.g.  $5.7 \pm 2.79$  Ma (Gradstein *et al.* 1995). If all 250 Domaro couplets in the lower cyclic interval were precession forced, the Domaro cyclic interval would be  $4.975 \pm 0.08$  Ma long, or would span a total *ca.* 10 subzones (i.e.  $4.975$  Ma/ $(0.468$  Ma/subzone)). The lowest firm biozone marker that we have in the Domaro at Colle di Sogno is at metre 60 (figure 2), with first occurrence (FO) of *Lotharingius primigenius* (E. Erba, unpublished data) in the lower *spinatum* zone (Cobianchi & Erba 1990). Thus, the youngest biozone that could be represented in the lower Domaro cyclic interval is most likely the *gibbosus* subzone; counting downward 10 subzones brings us to the Middle Carixian, in the *jamesoni* subzone, or, using the Pliensbachian subzone cyclochronologic estimates of Weedon & Jenkyns (1999), in the *polymorphus* subzone. Finally, according to Torri (L. Torri, personal communication), the top of the Sinemurian occurs only metres below the base of the measured cyclic interval.

The only well-constrained boundaries of the Sogno Formation are at the basal Pliensbachian–Toarcian boundary and at the Aalenian–Bajocian boundary at the top, which have radiometric ages of  $189.6 \pm 2.0$  Ma and  $176.5 \pm 2.0$  Ma, respectively (Gradstein *et al.* 1995). This gives a duration of  $13.1 \pm 2.8$  Ma for the combined Toarcian–Aalenian stages. We have developed a cyclochronologic estimate for this duration as follows. For the 278 obliquity cycles over metres 16–130.0 and assuming a 37.0 ka average Middle Jurassic (180 Ma) obliquity period (Berger *et al.* 1992), this implies a duration of 10.286 Ma for the interval. If obliquity cycles maintain a 7% standard deviation in periodicity back through time, then over these  $N = 278$  Sogno obliquity cycles, the nominal standard deviation of this duration estimate follows  $\sigma N^{-0.5}$ , i.e. is 0.4%, or  $\pm 0.04$  Ma. For metres 0–16, we can only assume an average accumulation rate for the covered black shale, using our interpretation of precession cycles for the 30 cm cycle thicknesses from metres 4 to 8. This gives an accumulation rate of  $1.5 \text{ cm ka}^{-1}$ , which over the 16.2 m interval gives a duration of 1.080 Ma. Presumably 54 precession cycles (with 15% standard deviations) would have been completed over this interval, giving a 2% standard deviation for this estimate, or  $\pm 0.022$  Ma. Thus, the combined duration of the Toarcian and Aalenian stages is  $11.37 \pm 0.05$  Ma. The potential for unrecorded cycles due to stratigraphic gaps makes this a minimum estimate for the interval. Other ‘noise’ elements related to biased sampling and preservation of the fossils, also inaccuracies in the stratigraphic correlation to the standard stage boundaries, are not accounted for in this estimate, and unfortunately are likely to be significant enough to swamp the above-quoted uncertainties.

The Sogno biozones in figure 2 were assigned according to the FOs of fossils, and so their true ranges in the section are open to revision. Using the radiometric chronologies provided, we propose that the Toarcian–Aalenian boundary may instead occur at Sogno cycle no. 181 (counting 97 obliquity cycles down from the Aalenian–Bajocian boundary), or at metre 103.4. This position coincides with the start of Lithozone 3 originally proposed by Gaetani & Poliani (1978) to demarcate an increase in radiolarian chert in the section. Also, the Sogno biozonation used *Discorhabdus striatus* FO in the *opalinum* zone, after Cobianchi & Erba (1990), which has recently been revised as first occurring in the somewhat older *bifrons* zone (Picotti & Cobianchi 1996). The new high-precision Middle Toarcian (*variabilis* zone) date of Palfy *et al.* (1997) would then occur 132 obliquity cycles down from the Aalenian–Bajocian boundary, or at metre 90.9. This date of  $181.4 \pm 0.6$  Ma is precise to roughly an interval of  $\pm 600 \text{ ka}/(37 \text{ ka}) = \pm 16$  cycles, or  $\pm 5$  m within metre 90.9 (although standard deviations also have uncertainties associated with them).

## 7. Conclusions

The Pliensbachian–Bajocian thin bedded basinal carbonate cycles from the Lombard Basin of the Southern Alps show evidence of orbital insolation forcing. Analysis was performed by a frequency modulation analysis of the cycles and comparison with frequency modulation characteristics of model orbital signals. These observations provided *a priori* information for then developing incremental time-scales over segments of the section to evaluate the sedimentary signal directly.

The results show that the Pliensbachian limestone–shale couplets of the Domaro Limestone contain a dual-component signal that closely resembles that of the pre-

cession. The overlying Toarcian–Bajocian Sogno Formation cycles in contrast underwent a series of basic frequency changes, which ultimately involved a fundamental change in cyclicity to a largely single-component signal with frequency modulations resembling that of obliquity.

The origin of this cyclicity in Jurassic carbonate accumulation is proposed to be due to metre-scale sea-level oscillations forced by orbital insolation acting on continental water and/or ice reservoirs. The varying sea-levels dictated carbonate productivity on platform environments and the exportation of the finer (mud) fraction into the surrounding deep seas. The switch to a pure obliquity signal in the Middle Toarcian Sogno Formation requires that equal amounts of landlocked water responded to insolation similarly in both the Northern and Southern Hemispheres, so that the precession component became counterphased and suppressed in the eustatic response, while obliquity was reinforced. This apparently occurred also during the Pliocene when glaciation intensified in the Northern Hemisphere, and ice volumes approached those in Antarctica.

The evidence for orbital forcing allowed us to develop a cyclochronology for the Colle di Sogno Section. Counting obliquity-forced Sogno cycles indicates a minimum duration of  $11.37 \pm 0.05$  Ma for the combined Toarcian–Aalenian stages, which compares well with the radiometric estimate of  $13.1 \pm 2.8$  Ma from Gradstein *et al.* (1995). This cyclochronologic estimate is open to revision pending further investigation of cyclic processes in the Lower Toarcian black shale interval, which could not be accessed at Colle di Sogno. The limestone–shale couplet succession of the underlying Pliensbachian Domaro Limestone has frequency characteristics that are remarkably like those of the multicomponent precession, although unfortunately, the lower boundary of this sequence is not biostratigraphically constrained. Using an equal Hettangian–Bajocian ammonite subzone chron assumption, we estimate a cyclochronology for all of the 250 Domaro couplets of  $4.975 \pm 0.022$  Ma, and propose that the lower boundary of the Domaro Limestone at Colle di Sogno lies in the Middle Carixian (the *jamesoni* subzone, within the *jamesoni* zone).

We thank Dr Elisabetta Erba of the University of Milan and Dr Miriam Cobianchi of the University of Pavia for sharing with us their work on the nannofossil stratigraphy of the Sogno Formation and the Liassic–Dogger Lombardian Basin, and we apologize for any errors in our placement of biozone boundaries in figure 2. We are grateful to Sir Nicholas Shackleton and Professor André Berger, who during the London Discussion motivated us to devise the approach presented in this paper. We also sincerely thank Dr Marie-France Loutre, who clarified numerous points on orbital theory for us. Finally, we very much appreciated the careful reviews by Dr Graham Weedon, Professor Walther Schwarzacher, and Professor Nick McCave, which resulted in substantial improvements to the final version of this paper. L.H. was supported by the Petroleum Research Fund of the American Chemical Society (grant no. 21119-AC8), and by student grants from the Geological Society of America, the Sigma Xi Society, and the Johns Hopkins University Balk Field Fund.

## References

- Baumgartner, P. O. 1987 Age and genesis of Tethyan Jurassic Radiolarites. *Eclogae Geologicae Helvetiae* **80**, 831–879.
- Berger, A. 1978 A simple algorithm to compute long term variations of daily or monthly insolation. Contribution no. 18, Institut d'Astronomie et de Géophysique Georges LeMaitre, Université Catholique de Louvain, Louvain-la-Neuve, Belgium.

*Phil. Trans. R. Soc. Lond. A* (1999)

- Berger, A. & Loutre, M. F. 1990 Origine des fréquences des éléments astronomiques intervenant dans le calcul de l'insolation. *Bull. Classes Sci. Acad. R. Belgique* **1**, 45–106.
- Berger, A. & Loutre, M. F. 1994 Astronomical forcing through geological time. In *Orbital forcing and cyclic sequences* (ed. P. L. de Boer & D. G. Smith), pp. 15–24. International Association of Sedimentologists Spec. Publ. no. 19. Blackwell Scientific.
- Berger, A., Loutre, M.-F. & Laskar, J. 1988 Insolation values for the climate of the last 10 Myr. Université Catholique de Louvain, Institut d'Astronomie et de Géophysique Georges LeMaître, Université Catholique de Louvain, Louvain-la-Neuve, Belgium, Scientific Report 1988/13, 17 pp.
- Berger, A., Loutre, M.-F. & Laskar, J. 1992 Stability of the astronomical frequencies over the Earth's history for paleoclimatic studies. *Science* **255**, 560–565.
- Berger, W. H., Bickert, T., Wefer, G. & Yasuda, M. K. 1995 Brunhes–Matuyama boundary: 790 k.y. date consistent with ODP Leg 130 oxygen isotope records based on fit to Milankovitch template. *Geophys. Res. Lett.* **22**, 1525–1528.
- Bertotti, G., Picotti, V., Bernoulli, D. & Castellarin, A. 1993 From rifting to drifting: tectonic evolution of the South-Alpine upper crust from the Triassic to the Early Cretaceous. *Sedimentary Geol.* **86**, 53–76.
- Brack, P., Mundil, R., Meier, M., Oberli, F. & Rieber, H. 1996 Biostratigraphic and radiometric data question the Milankovitch characteristics of the Latemar cycles. *Geology* **24**, 371–375.
- Brack, P., Mundil, R., Meier, M., Oberli, F. & Rieber, H. 1997 Biostratigraphic and radiometric data question the Milankovitch characteristics of the Latemar cycles—Reply. *Geology* **25**, 471–472.
- Claps, M. 1993 *Ciclicità ad alta frequenza nella piattaforma carbonatica dei Calcari Grigi (Giurassico Inferiore, Pealpi Venete): evidenze di controllo eustatico*. Dottorato di Ricerca in Scienze della Terra, Università di Ferrara, Italy.
- Claps, M., Erba, E., Masetti, D. & Melchiorri, F. 1995 Milankovitch-type cycles recorded in Toarcian black shales from the Belluno Trough (Southern Alps, Italy). *Mem. Sci. Geol. It.* **47**, 179–188.
- Cobianchi, M. & Erba, E. 1990 Biostratigraphy of Jurassic calcareous nannofossils in the Lombard Basin. *Mem. Soc. Geol. It.* **45**, 150–151.
- Crevello, P. D. 1991 High-frequency carbonate cycles and stacking patterns: interplay of orbital forcing and subsidence on Lower Jurassic rift platforms, High Atlas, Morocco. In *Sedimentary modeling: computer simulations and methods for improved parameter definition* (ed. E. V. Franseen, W. L. Watney, C. G. St C. Kendall & W. Ross). Kansas Geological Survey Bulletin no. 233, pp. 207–230.
- Crowley, T. J., Kim, K.-Y., Mengel, J. G. & Short, D. A. 1992 Modeling 100,000 year climate fluctuations in pre-Pleistocene time series. *Science* **255**, 705–707.
- Deconinck, J.-F. & Bernoulli, D. 1991 Clay mineral assemblage of Mesozoic pelagic and flysch sediments of the Lombardian Basin (Southern Alps); implications for palaeotectonics, palaeoclimate and diagenesis. *Geologische Rundschau* **80**, 1–17.
- Delavenna, M. F., Steinberg, M., Trauth, N. & Holtzapffel, T. 1989 Influence des cycles eustatiques et de la tectonique synsédimentaire sur la minéralogie du Lias et du Dogger du forage de Sancerre-Couy (Cher). Programme Géologie profonde de la France. *C. R. Acad. Sci. Paris II* **308**, 111–116.
- Enos, P. 1991 Sedimentary parameters for computer modeling. In *Sedimentary modeling: computer simulations and methods for improved parameter definition* (ed. E. V. Franseen, W. L. Watney, C. G. St C. Kendall & W. Ross). Kansas Geological Survey Bulletin no. 233, pp. 63–100.
- Fischer, A. G. & Hinnov, L. A. 1997 Orbitally forced glaciations during greenhouse and icehouse times. Part 1. A global model. *Geol. Soc. Am.* (Abstracts with Programs) A-211.

- Frakes, L. A., Francis, J. E. & Syktus, J. I. 1992 *Climate modes of the Phanerozoic*. Cambridge University Press.
- Gaetani, M. 1975 Jurassic stratigraphy of the Southern Alps; a review. In *The geology of Italy* (ed. C. Squyres), pp. 377–402. Libyan Arab Republic Earth Sciences.
- Gaetani, M. & Poliani, G. 1978 Il toarciano et il giurassico medio in Albenza (Bergamo). *Riv. Ital. Paleont. Strat.* **84**, 349–382.
- Goldhammer, R. K., Dunn, P. A. & Hardie, L. A. 1987 High-frequency glacio-eustatic oscillations with Milankovitch characteristics recorded in Northern Italy. *Am. J. Sci.* **287**, 853–892.
- Goldhammer, R. K., Dunn, P. A. & Hardie, L. A. 1990 Depositional cycles, composite sea-level changes, cycle stacking patterns and the hierarchy of stratigraphic forcing: examples from the Alpine Triassic platform carbonates. *Geol. Soc. Am. Bull.* **102**, 535–562.
- Gomez, J. & Goy, A. 1999 Sequential analysis of the Toarcian in the northern central-eastern part of the Iberian Subplate (Spain). In *Proc. Fifth Int. Jurassic Symp. 1998, Vancouver, Canada*.
- Goy, J. (and 14 others) 1999 Integrated study of the Toarcian–Aalenian boundary at the Fuentelsaz section, Iberian Range (Spain). In *Proc. Fifth Int. Jurassic Symp. 1998, Vancouver, Canada*.
- Gradstein, F. M., Agterberg, F. P., Ogg, J. G., Hardenbol, J., Van Veen, P., Thierry, J. & Huang, Z. 1995 A Triassic, Jurassic and Cretaceous time scale. In *Geochronology, time scales and global stratigraphic correlation* (ed. W. A. Berggren, D. V. Kent, M. P. Aubry & J. Hardenbol). *SEPM* (Spec. Publ.) **54**, 95–126.
- Hallam, A. 1975 *Jurassic environments*. Cambridge University Press.
- Haq, B. U., Hardenbol, J. & Vail, P. R. 1988 Mesozoic and Cenozoic chronostratigraphy and eustatic cycles. In *Sea-level changes: an integrated approach* (ed. C. K. Wilgus, B. S. Hastings, C. G. St. C. Kendall, H. W. Posamentier, C. A. Ross & J. C. Van Wagoner). *SEPM* (Spec. Publ.) **42**, 71–108.
- Hardie, L. A. & Hinnov, L. A. 1997 Biostratigraphic and radiometric data question the Milankovitch characteristics of the Latemar cycles—comment. *Geology* **25**, 470–471.
- Herbert, T. D. 1992 Paleomagnetic calibration of Milankovitch cyclicity in Lower Cretaceous sediments. *Earth Planet. Sci. Lett.* **112**, 15–28.
- Herbert, T. D. 1994 Reading orbital signals distorted by sedimentation: models and examples. In *Orbital forcing and cyclic sequences* (ed. P. L. de Boer & D. G. Smith), pp. 483–508. International Association of Sedimentologists, Spec. Publ. no. 19. Blackwell Scientific.
- Hinnov, L. A. & Park, J. 1998 Detection of astronomical cycles in the sedimentary record using frequency modulation analysis. *J. Sediment. Res.* **68**, 325–338.
- Hinnov, L. A., Park, J. & Erba, E. 1999 Lower–middle Jurassic rhythmites from the Lombard Basin, Italy: a record of orbitally-forced cycles modulated by long-term secular environmental changes in west Tethys. In *Proc. Fifth Int. Jurassic Symp. 1998, Vancouver, Canada*.
- Jacobs, D. K. & Sahagian, D. L. 1995 Milankovitch fluctuations in sea level and recent trends in sea-level change: ice may not always be the answer. In *Sequence stratigraphy and depositional response to eustatic, tectonic and climatic forcing* (ed. B. Haq), pp. 329–366. Dordrecht, The Netherlands: Kluwer.
- Jenkyns, H. C. 1988 The early Toarcian (Jurassic) anoxic event: stratigraphic, sedimentary and geochemical evidence. *Am. J. Sci.* **288**, 101–151.
- Jenkyns, H. C. & Clayton, C. J. 1997 Lower Jurassic epicontinental carbonates and mudstones from England and Wales: chemostratigraphic signals and the early Toarcian anoxic event. *Sedimentology* **44**, 687–706.
- Jimenez, A. P., Jimenez de Cisneros, C., Rivas, P. & Vera, J. A. 1996 The Early Toarcian anoxic event in the westernmost Tethys (Subbetic): paleogeographic and paleobiogeographic significance. *J. Geol.* **104**, 399–416.

- Johnson, R. G. 1982 Brunhes/Matuyama magnetic reversal dated at 790,000 yr. B. P. by marine-astronomical correlation. *Quat. Res.* **17**, 135–147.
- Kälin, O. 1980 *Schizosphaerella punctulata* DEFLANDRE & DANGEARD: Wall infrastructure and preservation in deeper-water carbonate sediments of the Tethyan Jurassic. *Eclogae Geologicae Helvetiae* **73**, 983–1008.
- Laskar, J. 1990 The chaotic motion of the Solar System: a numerical estimate of the size of the chaotic zones. *Icarus* **88**, 266–291.
- Mankinen, E. A. & Dalrymple, G. B. 1979 Revised geomagnetic polarity time scale for the interval 0–5 M.y. B.P. *J. Geophys. Res.* **84**, 615–626.
- Masetti, D., Claps, M., Avanzini, M., Giacometti, A. & Pignatti, P. 1996 I Calcari Grigi della Piattaforma di Trento. *78a Riunione Estiva, Geologia delle Dolomiti*. San Cassiano, Italy: Società Geologica Italiana.
- Montanari, L. 1974 Contributo all conoscenza del Domeriano nelle Prealpi Lombarde. *Soc. Geol. It. Mem.* **132**, 241–249.
- Palfy, J., Parrish, R. R. & Smith, P. L. 1997 A U–Pb age from the Toarcian (Lower Jurassic) and its use for time scale calibration through error analysis of biochronologic dating. *Earth Planet. Sci. Lett.* **146**, 659–675.
- Picotti, V. & Cobianchi, M. 1996 Jurassic periplatform sequences of the eastern Lombardian Basin (southern Alps): the deep-sea record of the tectonic evolution, growth and demise history of a carbonate platform. *Mem. Sci. Geol.* **48**, 171–219.
- Podlaha, O. G., Mutterlose, J. & Veizer, J. 1998 Preservation of  $\delta^{18}\text{O}$  and  $\delta^{13}\text{C}$  in belemnite rostra from the Jurassic/Early Cretaceous successions. *Am. J. Sci.* **298**, 324–347.
- Sarti, M., Bosellini, A. & Winterer, E. L. 1992 Basin geometry and architecture of a Tethyan passive margin, Southern Alps, Italy: implications for rifting mechanisms. In *Geology and geophysics of continental margins* (ed. J. S. Watkins, Z. Feng & K. J. McMillen). *AAPG Mem.* **53**, 241–258.
- Schwarzacher, W. 1964 An application of statistical time-series analysis of a limestone/shale sequence. *J. Geol.* **72**, 195–213.
- Schwarzacher, W. & Fischer, A. G. 1982 Limestone-shale bedding and perturbations of the Earth's orbit. In *Cycle and event stratification* (ed. G. Einsele & A. Seilacher), pp. 72–95. New York: Springer.
- Shackleton, N. J., Berger, A. & Peltier, W. R. 1990 An alternative astronomical calibration of the Lower Pleistocene timescale based on ODP Site 677. *Trans. R. Soc. Edinb.* **81**, 251–261.
- Spell, T. L. & McDougall, I. 1992 Revisions to the age of the Brunhes–Matuyama boundary and the Pleistocene geomagnetic polarity timescale. *Geophys. Res. Lett.* **19**, 1181–1184.
- Thomson, D. 1982 Spectrum estimation and harmonic analysis. *IEEE Proc.* **70**, 1055–1096.
- Tintori, A. 1977 Toarcian fishes from the Lombardian Basin. *Boll. Soc. Paleontologica It.* **16**, 143–152.
- Vakhrameev, V. A. 1991 *Jurassic and Cretaceous floras and climates of the Earth*. Cambridge University Press.
- Valdes, P. J., Sellwood, B. W. & Price, G. D. 1995 Modelling Late Jurassic Milankovitch climate variations. In *Orbital forcing timescales cyclostratigraphy* (ed. M. R. House & A. S. Gale). *Geol. Soc. (Spec. Publ.)* **85**, 115–132.
- Van Buchem, F. S. P., McCave, I. N. & Weedon, G. P. 1994 Orbitally induced small-scale cyclicity in a siliciclastic epicontinental setting (Lower Lias, Yorkshire, UK). In *Orbital forcing and cyclic sequences* (ed. P. L. de Boer & D. G. Smith), pp. 345–366. International Association of Sedimentologists, Spec. Publ. no. 19. Blackwell Scientific.
- Weedon, G. P. 1989 The detection and illustration of regular sedimentary cycles using Walsh power spectra and filtering, with examples from the Lias of Switzerland. *J. Geol. Soc. Lond.* **146**, 133–144.

- Weedon, G. P. & Jenkyns, H. 1999 Cyclostratigraphy and the Early Jurassic time scale: data from the Belemnite Marls, Dorset, southern England. *Geol. Soc. Am. Bull.* (In the press.)
- Wigley, T. M. L. & Raper, S. C. B. 1987 Thermal expansion of sea water associated with global warming. *Nature* **330**, 127–131.
- Winterer, E. L. & Bosellini, A. 1981 Subsidence and sedimentation on a Jurassic passive continental margin, Southern Alps, Italy. *Am. Ass. Petrol. Geologists Bull.* **65**, 394–421.
- Zempolich, W. G. 1993 The drowning succession in Jurassic carbonates of the Venetian Alps, Italy: a record of supercontinent breakup, gradual eustatic rise, and eutrophication of shallow-water environments. In *Carbonate sequence stratigraphy: recent developments and applications* (ed. R. G. Loucks & J. F. Sarg). *Am. Ass. Petrol. Geologists Mem.* **57**, 63–105.

—

—

—

—

|

|